L_1 Adaptive Control Design for NASA AirSTAR Flight Test Vehicle

Irene M. Gregory[1]
NASA Langley Research Center, Hampton, VA 23681-2199, USA

Chengyu Cao[2]
University of Connecticut, Storrs, CT 06269

Enric Xargay[3] and Naira Hovakimyan[4]
University of Illinois at Urbana-Champaign, Urbana, Illinois 61801

Xiaotian Zou[5]
University of Connecticut, Storrs, CT 06269

In this paper we present a new L_1adaptive control architecture that directly compensates for matched as well as unmatched system uncertainty. To evaluate the L_1 adaptive controller, we take advantage of the flexible research environment with rapid prototyping and testing of control laws in the Airborne Subscale Transport Aircraft Research system at the NASA Langley Research Center. We apply the L_1 adaptive control laws to the subscale turbine powered Generic Transport Model. The presented results are from a full nonlinear simulation of the Generic Transport Model and some preliminary pilot evaluations of the L_1 adaptive control law.

I. Introduction

One of the primary objectives of the Integrated Resilient Aircraft Control (IRAC) Project, under the auspices of the Aviation Safety Program, is to advance the state of the art in the adaptive control technology. Of particular interest is piloted flight under adverse conditions such as unusual attitudes, surface failures and structural damage. The IRAC Project is using subscale flight testing as an important tool in the evaluation of experimental adaptive control laws. This is particularly beneficial for the test and evaluation of control law performance beyond the edge of the normal flight envelope, where the risk of vehicle loss is high due to limited knowledge of nonlinear aerodynamics beyond stall and the potential for high structural loads. The Airborne Subscale Transport Aircraft Research (AirSTAR)[1-6] system at the NASA Langley Research Center has been designed to provide a flexible research environment with the ability to conduct rapid prototyping and testing for control algorithms in extremely adverse flight conditions. We are exploiting this capability for an in-depth look at various aspects of adaptive control pertinent to piloted dynamically scaled turbine powered aircraft. In this paper we present a new L_1 adaptive

---

[1] Senior Research Engineer, Dynamic Systems and Control Branch, AIAA Senior Member
[2] Assistant Professor, Department of Mechanical Engineering, AIAA Member
[3] Graduate Student, Department of Aerospace Engineering, AIAA Student Member
[4] Professor, Department of Mechanical Science and Engineering, AIAA Associate Fellow
[5] Graduate Student, Department of Mechanical Engineering, AIAA Member

control architecture that directly compensates for matched as well as unmatched system uncertainty. We apply the new L_1 adaptive control laws to the subscale turbine powered Generic Transport Model (GTM).

The L_1 adaptive control architecture was first proposed by Cao and Hovakimyan[7-10] and applied to a wide variety of flight vehicles over the last couple of years[11-14]. In this paper we present a theoretical extension of the L_1 adaptive control that accounts for matched as well as *unmatched* dynamic uncertainty. An earlier output feedback formulation of the L_1 adaptive control that accounted for unmatched uncertainties has been presented in reference 15. Unlike conventional adaptive controllers, the L_1 controller adapts fast, leading to desired transient and asymptotic tracking with guaranteed, bounded away from zero, time-delay margin. These features of the L_1 control theory make it an excellent candidate for validation and verification (V&V) purposes.

We apply this extended state feedback L_1 architecture to a dynamically scaled jet powered remotely piloted aircraft, the GTM, with the control objective to achieve tracking for a variety of tasks with guaranteed stability and robustness in the presence of uncertain dynamics, such as changes due to rapidly varying flight conditions during standard maneuvers, and unexpected failures. The control system presented here is a three axis angle of attack (AOA or α), roll rate (p) – sideslip angle (β) command augmentation system (CAS). Specific cases presented in this paper include angle of attack capture for pre-stall, stall, post-stall and high α, mid-range angle of sideslip (β) capture, and large roll rate (p) doublet command following. These tasks are simulated for a variety of damage and failure conditions described in detail later in the paper. Furthermore, we present some preliminary pilot evaluation results for aircraft of varying stability and some additional maneuvers. The simulation of the GTM aircraft contains full nonlinear, asymmetric aerodynamics[16], actuator dynamics, sensor dynamics including noise, and other nonlinear elements typical of high fidelity aircraft simulations.

The paper is organized as follows. Section II provides a brief AirSTAR flight test facility overview with emphasis on flight control law implementation environment. In section III, we present the development of the L_1 adaptive control three axes α, p-β CAS. Section IV describes the results from simulated scenarios and some preliminary piloted evaluation tasks. Section V presents concluding remarks and describes our future research plans.

II. AirSTAR Overview

AirSTAR is an integrated flight test infrastructure which utilizes remotely piloted, jet powered subscale models for flight testing. One particular use of AirSTAR is flight testing research control laws in adverse flight conditions. AirSTAR consists of a remotely piloted subscale test article, the Mobile Operations Station (MOS) (an integrated ground station and control room), and a test range. Description of AirSTAR Concept of Operations can be found in references 1-3. Basically, the research pilot executes a flight test plan from a research cockpit located in the MOS, which utilizes synthetic vision displays driven with aircraft sensor data. The research pilot uses a ground-based flight control system (FCS) that is connected to the aircraft through a telemetry link.

A. AirSTAR Infrastructure

Currently, AirSTAR's primary test aircraft is a 5.5% dynamically scaled twin-turbine powered generic transport model (GTM) shown in Fig 1. Dynamic scaling (i.e., similitude using equal Froude number and relative density between model-scale and full-scale) allows subscale flight test results to be applied to full-scale aircraft. This model (tail number T2) has a 6.5 ft wingspan, weighs 54 lbs at takeoff, and has a flight time of approximately 12 minutes. The aircraft is outfitted with full flight test instrumentation, including angle of attack and angle of sideslip vanes, sensors measuring static and dynamic pressure, control surface positions, rate gyros and accelerometers, a 6-DOF INS/GPS package, and engine instrumentation. Downlink data update rates vary from 5 Hz on the GPS data to 200 Hz on the data from analog sensors. Uplink commands are received at 200 Hz.

Figure 1. AirSTAR Test Aircraft

The GTM aircraft has been extensively tested in the NASA Langley wind tunnels with particular emphasis on modeling nonlinear regions of the extended flight envelope well beyond nominal flight as well as developing a database for a number of structural damage scenarios[16,17,18]. The high fidelity nonlinear simulation of the GTM aircraft, built up from the extensive wind tunnel data, has been incorporated into the AirSTAR facility. With this capability AirSTAR provides research environment where all variables are the same except one – the research pilot is either flying a real GTM aircraft or its high fidelity model. We take advantage of this similitude between simulation and flight test in developing out $\mathcal{L}_1$ adaptive control laws for flight test on the GTM aircraft.

B. AirSTAR Flight Control System Structure

Of particular relevance to this paper is the flight control system development and implementation in the AirSTAR facility. The flight control system (FCS) is developed in The MathWorks MATLAB®/Simulink® environment and implemented on a ground-based dSPACE® real-time computer located in the MOS. Detailed description of the flight control system software development and implementation can be found in references 2 and 3. A block diagram of the ground based flight software is provided for reference in Fig. 2. The commands from both pilots are input to the FCS, in addition to the aircraft sensor data, the output from the Calculated Parameters subsystem, and the Caution & Warning subsystem. The Calculated Parameters subsystem calculates unmeasured quantities such as airspeed and altitude (from dynamic and static pressure) and applies center of gravity offset corrections to appropriate sensor data.

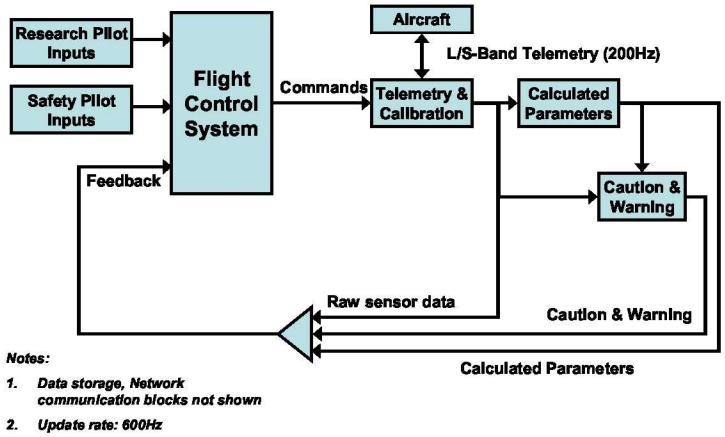

Figure 2. Block diagram of ground-based flight software.

The top level flight control system block diagram is depicted in Fig.3. It is important to note that the T2 aircraft has split surfaces - 4 elevator segments, inboard/outboard, left/right, right/left aileron, 2 rudder segments, upper/lower, flaps and spoilers. Segmented surfaces allow a range of failure emulation that go beyond surface failures and include aerodynamic stability variations. The research flight control law (FCL) resides in Mode 3 FCL module, which can contain any number of control laws, though only one can be operational at any one time. Furthermore, the current operational research flight envelope for the T2 Model, enforced by the loads protection system, is $600 \le Alt \le 1500$ ft and $40 \le V \le 120$ KEAS.

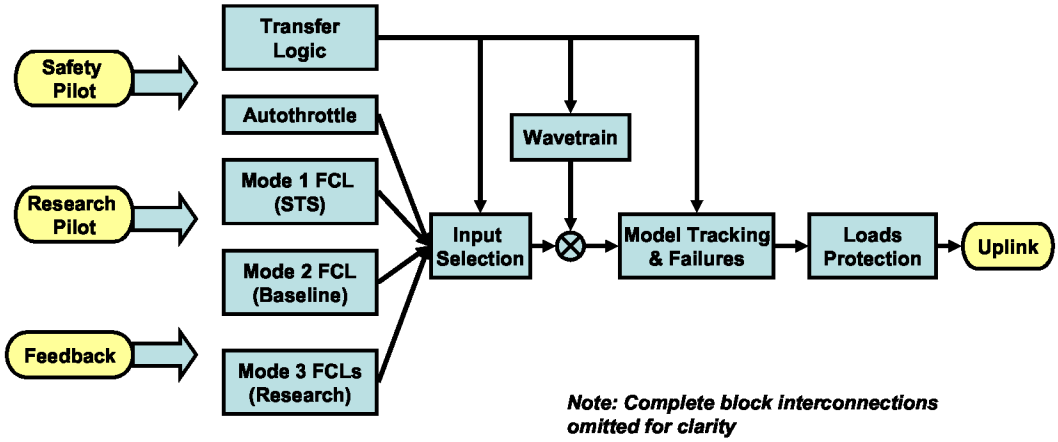

Figure 3. AirSTAR FCS top-level block diagram.

While we are preparing to go to flight test with the L_1 adaptive control laws, in this paper we primarily report results from nonlinear simulation under variety of conditions and some preliminary piloted evaluation tasks.

III. L_1 adaptive control laws for the GTM

The research control law developed for the GTM aircraft has as its primary objective achieving tracking for a variety of tasks with guaranteed stability and robustness in the presence of uncertain dynamics, such as changes due to rapidly varying flight conditions during standard maneuvers, and unexpected failures. All of this must be achieved while providing good handling qualities under nominal as well as adverse conditions. The L_1 control system presented here is a three axes angle of attack (AOA or α), roll rate (p) – sideslip angle (β) command augmentation system (CAS).

The simulation model is a full highly nonlinear coupled dynamic simulation, as previously mentioned. However, the desired control system quality is to provide a decoupled response between longitudinal and lateral-directional axis, as well as, between lateral and directional axis as much as possible. The longitudinal α-command response type was chosen for two reasons. One, the operational baseline control law is α-command so the same response would make direct control law comparison relevant. And more importantly, other research tasks performed on the GTM require precise α control. However, α-command control law brings its own challenges to adaptive control formulation. In addition, the phugoid mode of the dynamically scaled aircraft is much closer in frequency to the short period dynamics. The combination of α-command response type and faster phugoid dynamics result in a significant level of unmatched uncertainties. In a typical aircraft, without direct lift devices, control acts through moment generating effectors which implies that matched uncertainty propagates through moment equations of motion and any uncertainty in α would generate unmatched uncertainty. The lateral-directional p-β command augmentation system (CAS) is one of the standard response types.

Previous implementations of adaptive control in flight, whether JDAM missile[19,20] or UAV[11,21], have been as an augmentation to the existing baseline controller. There are a number of excellent reasons for this type of implementation. However, since we were designing a research control law for flight test, we had a great deal of interest in seeing what adaptation can do as a standalone. With a well designed robust baseline controller it is more difficult to assess how much adaptation is helping in providing stability and performance robustness, how much is the baseline controller contributing. Furthermore, we were interested in seeing how well our proposed L_1 architecture can handle significant unmatched uncertainties. Consequently the design presented here is a standalone L_1 adaptive controller introduced below[22].

A. Problem formulation:

Consider the following system dynamics:

$$\begin{aligned}
&\dot{x}(t) = A_m x(t) + B_m\left(u(t) + f_1\left(x(t), z(t), t\right)\right) + B_{um} f_2\left(x(t), z(t), t\right), \quad x(0) = x_o \\
&z(t) = g_0\left(x_z(t), t\right) \\
&\dot{x}_z(t) = g\left(x_z(t), x(t) t\right), \qquad x_z(0) = x_{zo} \\
&y(t) = cx(t),
\end{aligned} \tag{1}$$

where $x(t) \in \mathbb{R}^n$ is the system state vector (measured); $u(t) \in \mathbb{R}^m$ is the adaptive control signal; $y(t) \in \mathbb{R}^m$ is the regulated output; A_m is a known Hurwitz $n \times n$ matrix that defines the desired dynamics for the closed-loop system; $B_m \in \mathbb{R}^{n \times m}$ is a known constant matrix; $B_{um} \in \mathbb{R}^{n \times (n-m)}$ is a constant matrix such that $B_m^T B_{um} = 0$ and also $rank\left(\left[B_m \quad B_{um}\right]\right) = n$; $C \in \mathbb{R}^{m \times n}$ is a known constant matrix; $z(t)$ and $x_z(t)$ are the output and the state vector of internal unmodeled dynamics; $f_1(\cdot), f_2(\cdot), g_0(\cdot)$ and $g(\cdot)$ are unknown nonlinear functions. In this problem formulation, $f_1(\cdot)$ represents the matched component of the uncertainties, whereas $B_{um} f_2(\cdot)$ represents the unmatched component.

The above defined system needs to verify the following assumptions:

Assumption 1 *The unmodeled internal dynamics are BIBO stable.*

Assumption 2 *The nonlinear functions f_1 and f_2 are assumed to be semiglobally Lipschitz with respect to $x(t)$ and $z(t)$ uniformly in t.*

Assumption 3 *The partial derivatives of the nonlinear functions f_1 and f_2 with respect to $x(t)$, $z(t)$, and t are assumed to be semiglobally uniformly bounded.*

Assumption 4 *The transmission zeros of the transfer matrix from the control input $u(t)$ to the output of the system $y(t)$ lie on the open left-half plane.*

Then, the control objective is to design an adaptive state feedback control law $u(t)$ to compensate for the effect of both the matched and unmatched uncertainties on the output of the system $y(t)$, and ensure that $y(t)$ tracks the output response of a *desired system* to a given bounded reference signal $r(t)$ *both in transient and steady-state*, while all other signals remain bounded.

B. L_1 Adaptive Controller for Unmatched Uncertainties

The elements of the L_1 adaptive control architecture are introduced below.

State predictor: We consider the following state predictor

$$\begin{aligned}\dot{\hat{x}}(t) &= A_m\hat{x}(t) + B_m\left(u(t)+\hat{\sigma}_m(t)\right) + B_{um}\hat{\sigma}_{um}(t), \qquad \hat{x}(0) = x_0\\ \hat{y}(t) &= C\hat{x}(t)\end{aligned} \tag{2}$$

where the adaptive estimates $\hat{\sigma}_m(t)$ and $\hat{\sigma}_{um}(t)$ are governed by the following adaptation laws.

Adaptive laws: Given $T_s > 0$, we define the adaptation for $\hat{\sigma}_m(t)$ and $\hat{\sigma}_{um}(t)$ as

$$\hat{\sigma}_m(t) = \hat{\sigma}_m(iT_s), \quad \hat{\sigma}_{um}(t) = \hat{\sigma}_{um}(iT_s), \quad t \in \left[iT_s, (i+1)T_s\right]$$

$$\begin{bmatrix}\hat{\sigma}_m(iT_s)\\ \hat{\sigma}_m(iT_s)\end{bmatrix} = -\left[\begin{array}{cc|c} \mathrm{I}_m & 0 & \\ 0 & \mathrm{I}_{n-m} & \end{array}\right]\left[B_m \quad B_{um}\right]^{-1}\Phi^{-1}(T_s)e^{A_mT_s}\tilde{x}(iT_s), \quad i = 1,2,3,\ldots \tag{3}$$

where

$$\Phi(T_s) = A_m^{-1}\left(e^{A_mT_s} - \mathrm{I}_n\right)$$

and $\tilde{x}(t) = \hat{x}(t) - x(t)$.

Control law: The control law is generated as

$$u(t) = u_m(t) + u_m(t) + K_g r(t) \tag{4}$$

where

$$\begin{aligned}u_m(s) &= -C_1(s)\hat{\sigma}_m(s)\\ u_{um}(s) &= -C_2(s)H_1^{-1}(s)H_2(s)\hat{\sigma}_{um}(s)\end{aligned}$$

with $H_1(s) = C\left(s\mathrm{I} - A_m\right)^{-1}B_m$ and $H_2(s) = C\left(s\mathrm{I} - A_m\right)^{-1}B_{um}$, while $K_g = -\left(CA_m^{-1}B_m\right)^{-1}$. $C_1(s)$ and $C_2(s)$ are low-pass filters with unity DC gain. $C_2(s)$ needs to ensure that $C_2(s)H_1^{-1}(s)H_2(s)$ is a proper transfer function. This choice for K_g ensures that the diagonal elements of the transfer matrix $\left[C\left(s\mathrm{I} - A_m\right)^{-1}B_mK_g\right]$ have DC gain equal to one, while the off-diagonal elements have zero DC gain.

C. L_1 Adaptive Controller for the GTM

The desired system dynamics for the GTM are decoupled and are given by

$$\begin{aligned}\dot{x}_m &= A_m x_m + B_m\delta_{cmd}\\ \begin{pmatrix}\dot{\alpha}\\ \dot{q}\end{pmatrix} &= \begin{pmatrix}\frac{Z_\alpha}{V} & 1+\frac{Z_q}{V}\\ M_\alpha & M_q\end{pmatrix}\begin{pmatrix}\alpha\\ q\end{pmatrix} + \begin{pmatrix}\frac{Z_\delta}{V}\\ M_{\delta_e}\end{pmatrix}\delta_e\end{aligned}$$

in the longitudinal axis for α-command and

$$\begin{pmatrix} \dot{p} \\ \dot{\beta} \\ \dot{r} \end{pmatrix} = \begin{pmatrix} L_p & 0 & 0 \\ 0 & Y_\beta / V & -1 \\ 0 & N_\beta & N_r \end{pmatrix} \begin{pmatrix} p \\ \beta \\ r \end{pmatrix} + \begin{pmatrix} L_{\delta a} & L_{\delta r} \\ Y_{\delta a} & Y_{\delta r} \\ N_{\delta a} & N_{\delta r} \end{pmatrix} \begin{pmatrix} \delta_a \\ \delta_r \end{pmatrix}$$

for the lateral-directional axis p-β command. We choose Hurwitz A_m and B_m such that the Level I handling qualities requirements[23] are satisfied. The low-pass filters $C_1(s)$ and $C_2(s)$, matched and unmatched uncertainty channels respectively, are chosen as first order and the bandwidth is adjusted based on the system dynamics.

The L_1 adaptive control laws were designed for a nominal system at V=80 KEAS and Alt = 1000 ft. The nominal GTM model has 22 msec time delay due to telemetry and sensor processing (6 msec on surface commands and 16 msec on sensor outputs). One further item of note, the L_1 adaptive controller was designed strictly for pilot in the loop flying, hence there is no outer loop compensation to hold altitude or pitch attitude. The results for a variety of test cases are presented in the next section.

IV. Results

The results presented in this section are two turbine-powered dynamically scaled GTM AirSTAR aircraft tail number T2. As mentioned previously the L_1 adaptive α, p-β command response control laws were designed for a nominal aircraft at a single flight condition (V=80 KEAS). The general maneuvers presented here include are based on high fidelity representation in simulation of damage cases tested in the wind tunnel as well as tasks expected to be evaluated in upcoming flight test.

A. Batch Simulation

To evaluate the stability and performance of the L_1 adaptive controller described in the previous section and designed at a single flight condition for a nominal aircraft, we have run a number of different cases simulating damage, failures, significant changes in vehicle stability, etc. We present a subset of these cases below to illustrate the stability and robust performance of the controller. We note that all variables presented below are measured quantities that contain sensor dynamics and measurement noise, this includes all actuator positions. We further note the range for actuator deflections: $-30 \le \delta e \le 20, -20 \le \delta a \le 20, -30 \le \delta r \le 30$. The actuator dynamics are very fast (300Hz) but the rate limits are included in the actuator dynamics nevertheless.

Case 1: Nominal aircraft

The first set of results show α command response to $\Delta\alpha$ = 3°, 6°, 9°. The initial condition at V=80 KEAS gives $\alpha_{trim} \approx 5.2°$ which results in $\alpha_{tot} \approx 8°, 11°, 14°$. For the GTM stall occurs at $\alpha \approx 11°$; $\alpha \approx 14°$ is post stall where there is a significant pitch break, pitch damping varies rapidly towards instability and is a function of pitch rate (q). All but the first response are for a highly nonlinear system. These α responses and their accompanying elevator deflections are superimposed on a single plot for easier comparison (Fig. 4). Note the α responses are all first order and scale according to the commanded α in pre-stall, stall and post-stall regions. The roll rate (p_{cmd} = 80deg/s) and β (β_{cmd}=6°) responses are provided as for future reference.

A similar exercise was completed with roll rate (p) for a very aggressive set of doublets – p_{cmd} = 80, 100, 120 deg/sec (Fig. 5). The roll rate response is very snappy and is limited only by aileron saturation which is especially noticeable for p_{cmd}=120deg/sec. Note that aileron saturation does not impact system stability and the roll rate response remains stable and predictable.

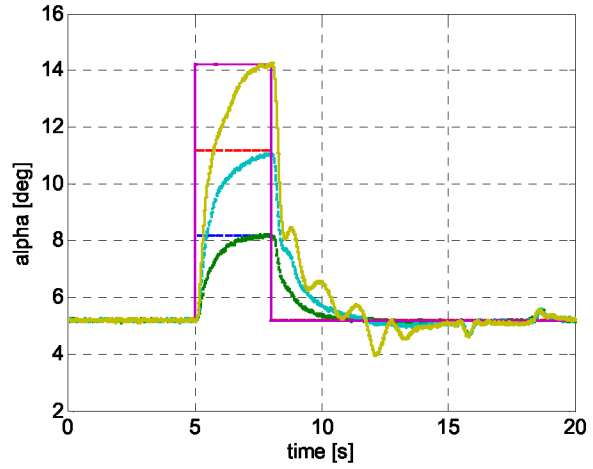

(a) Angle of attack

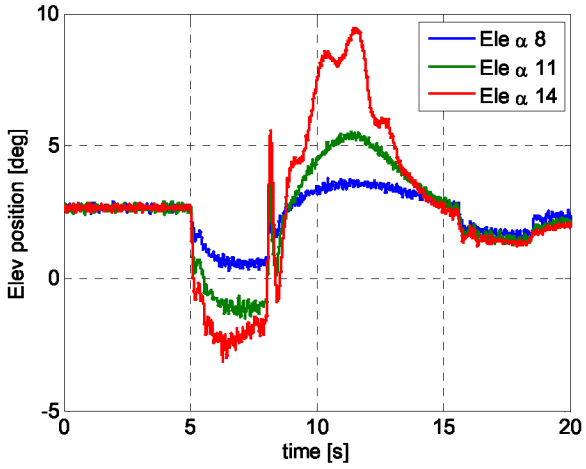

(b) Elevator

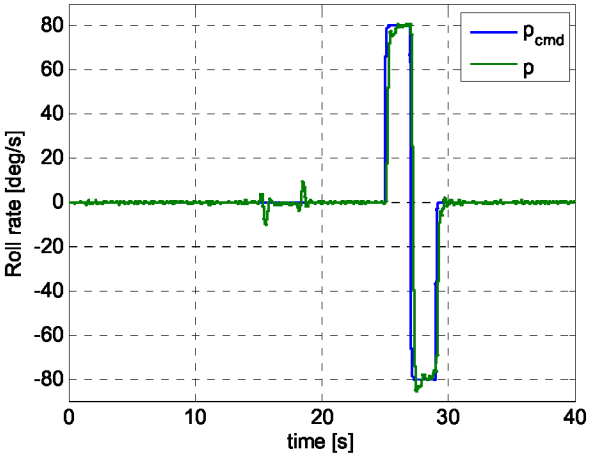

(c) Roll rate

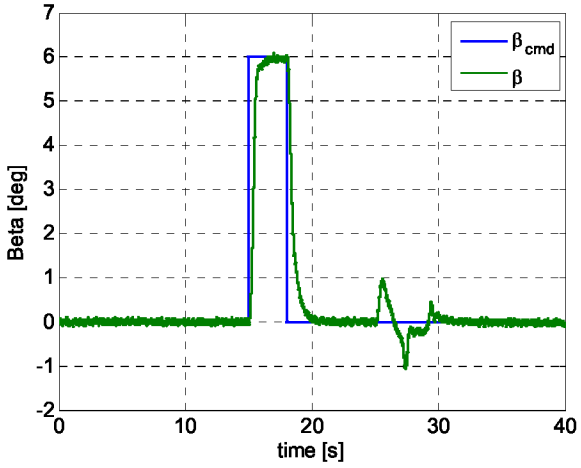

(d) Sideslip

Figure 4. Angle of attack response for $\alpha_{tot} \approx 8°$, at stall, $\alpha_{tot} \approx 11°$, and for post stall, $\alpha_{tot} \approx 14°$.

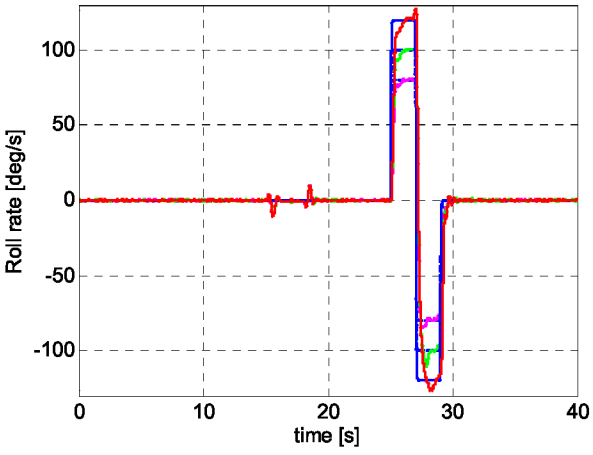

(a) Roll rate

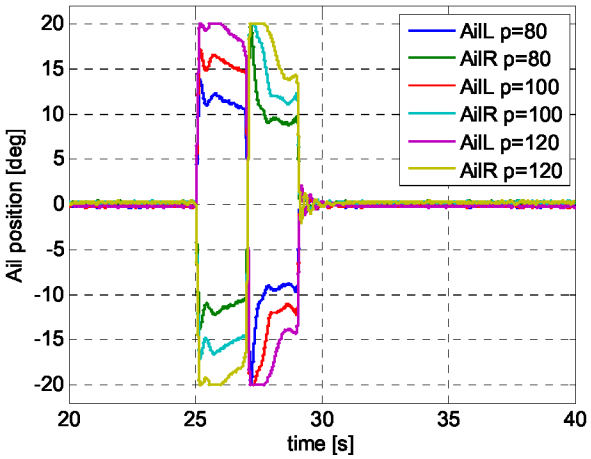

(b) Aileron

Figure 5. Roll rate response for p_{cmd} = 80, 100, 120 deg/sec

Case 2: Damage case – entire rudder missing

For this case, the primary aerodynamic effect is reduction in directional stability ($C_{n\beta}$); the primary control effect is complete loss in rudder control power (all effects due to rudder deflection go to zero). The dynamic effects are only provided for yaw rate, and only for the lateral/directional components, i.e., rolling moment, yawing moment, and side force due to body axis yaw rate. The simulation results are provided in Fig. 6.

The total loss of rudder results in inability of the aircraft to follow β_{cmd}=6° and β excursions of ≈ 2.5° when 80 deg/s roll rate is commanded. Furthermore, there is a slight bobble in α (α<1°) when roll rate is commanded. Roll rate command of 80 deg/sec is still achievable though the response does have slight oscillations. There is an attempt from the ailerons to compensate for the loss of the rudder and track β_{cmd}=6° while at the same time maintaining p_{cmd}=0. The result of these two competing actions is a small sustained roll rate for the duration of β command (Fig. 6 (c)-(d)).

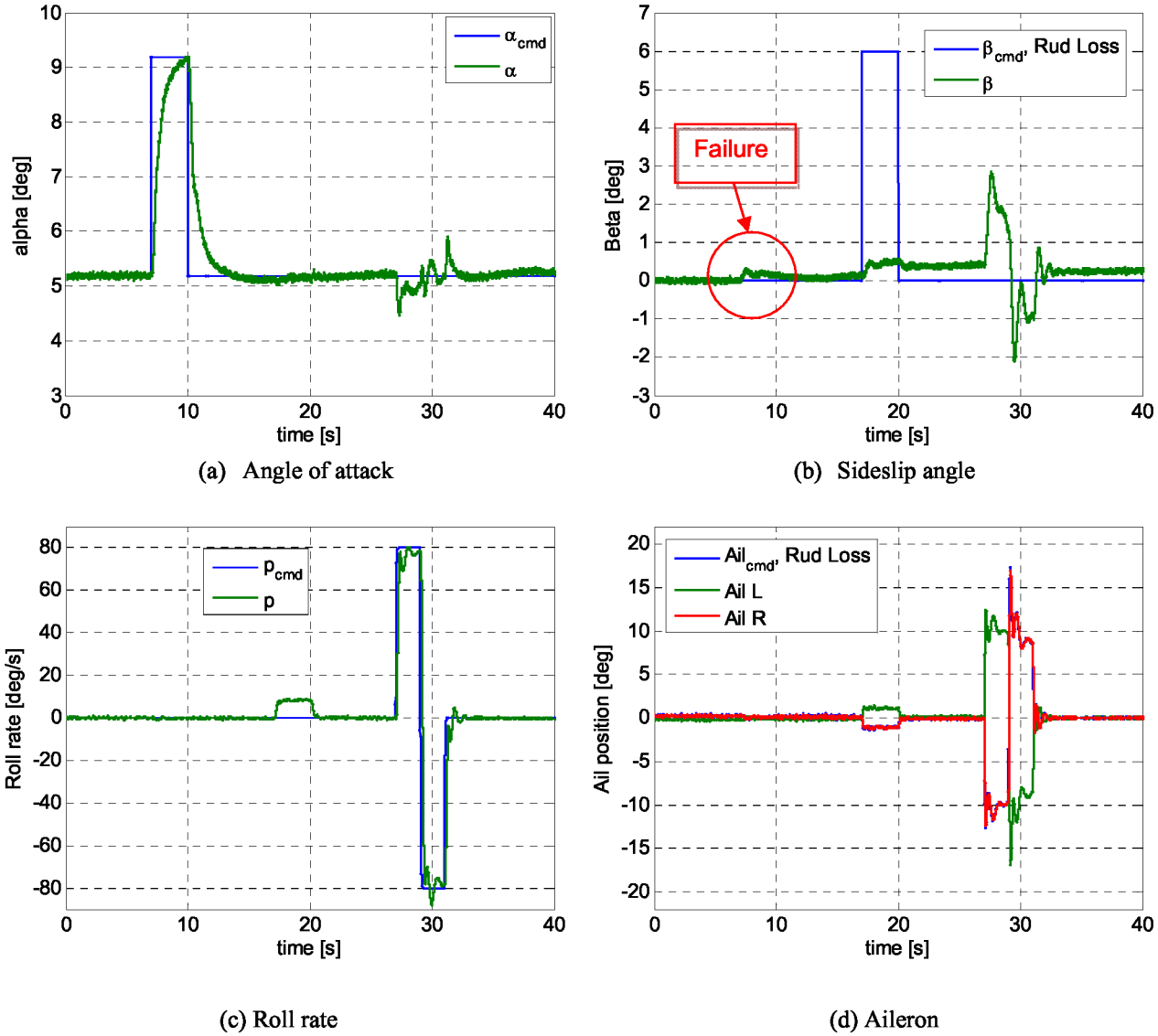

(a) Angle of attack

(b) Sideslip angle

(c) Roll rate

(d) Aileron

Figure 6. Missing rudder - α, p, β responses.

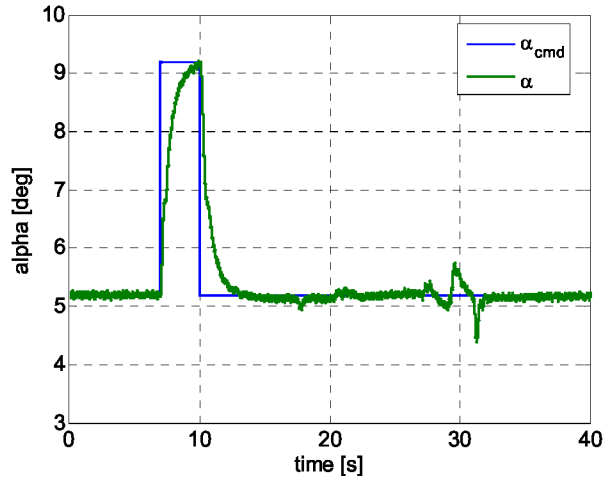

(a) Angle of attack

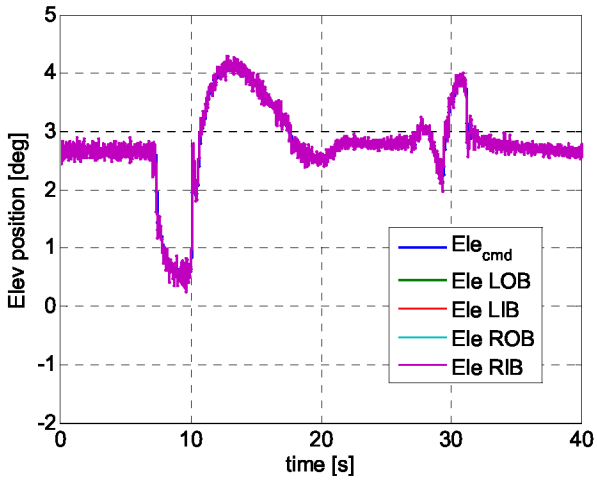

(b) Elevator

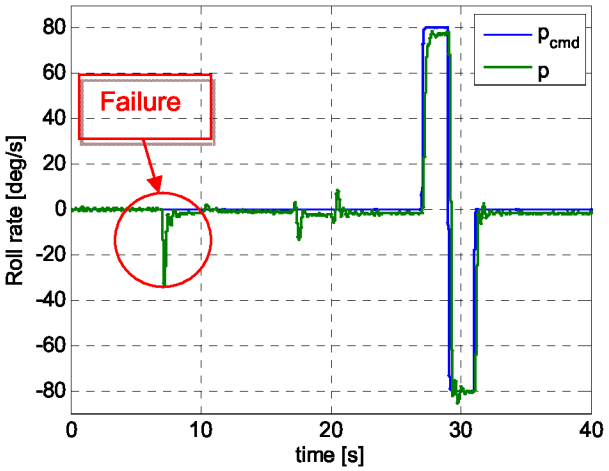

(c) Roll rate

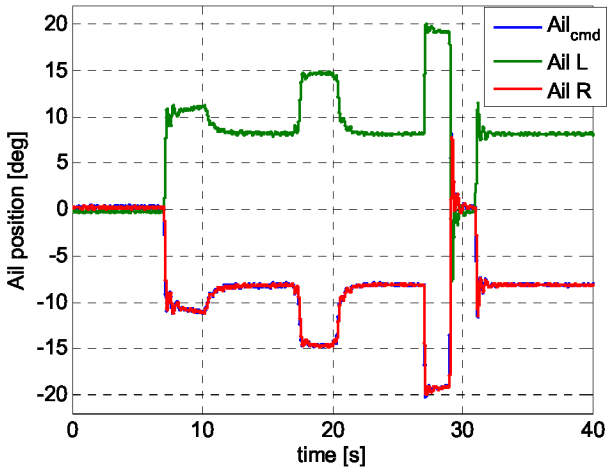

(d) Aileron

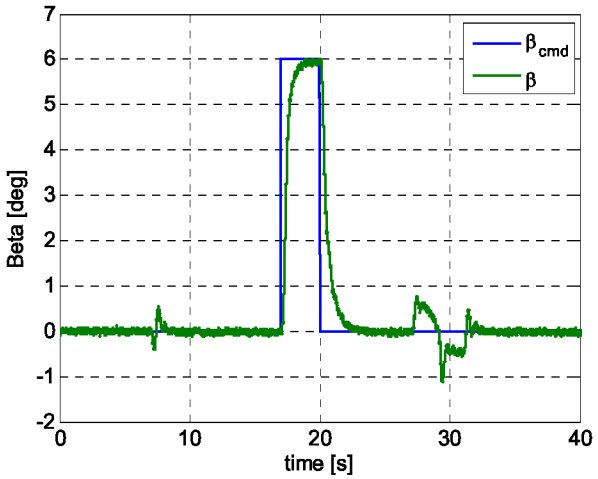

(e) Sideslip angle

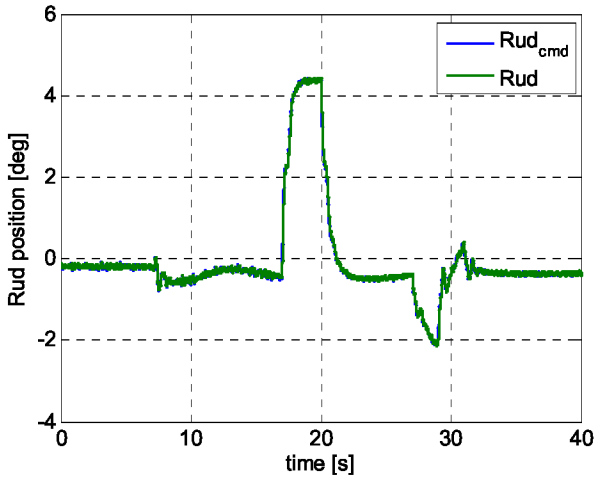

(f) Rudder

Figure 7. Missing left outboard trailing edge flap - α, p, β responses.

Case 3: Damage case – Left outboard trailing edge flap missing

The primary aerodynamic effect is rolling moment bias left wing down ($-\Delta Cl$), increases with alpha; the primary control effect is roll control required to compensate for roll asymmetry, thus available roll control power is reduced. The dynamic effects are only provided for roll rate, and only for the lateral/directional components, i.e., rolling moment, yawing moment, and side force due to body axis roll rate.

The L_1 adaptive controller response to the missing outboard trailing edge flap and resulting rolling moment is to use ailerons and a small rudder deflection to compensate as illustrated in Fig. 7. There is a minor impact on roll rate tracking, not enough control authority to reach 80 deg/sec. The α and β tracking performance is essentially unaffected.

Case 4: Damage case – Loss of outboard (approx 25% semispan) left wing tip

The primary aerodynamic effect is rolling moment bias left wing down ($-\Delta Cl$), which increases with α; the primary control effect is (i) left aileron now missing, thus all effects due to left aileron deflection go to zero, and (ii) roll control required to compensate for roll asymmetry, thus available roll control power is reduced. The dynamic effects are only provided for roll rate, and only for the lateral/directional components, i.e., rolling moment, yawing moment, and side force due to body axis roll rate.

The L_1 adaptive controller response to the loss of outboard left wing tip is provided in Fig. 8. While α tracking is not appreciably affected by the damage, the rolling moment increase as a function of α shows up in increased elevator activity to achieve α tracking. The right aileron and the rudder are used by the controller to compensate for the additional rolling moment and missing left aileron (deflection shown as zero magnitude). Roll rate tracking is the most affected in this damage case. There is insufficient control authority left, see saturated aileron in Fig. 8 (d), to achieve 80 deg/sec roll rate command tracking.

Case 5: Damage case 5 – Loss of entire elevator from left stabilizer

The primary aerodynamic effects are reduction in longitudinal stability and rolling moment bias left wing down ($-\Delta Cl$), increases with α; the primary control effect is (i) reduction in pitch control power, all effects due to left elevator deflection go to zero, (ii) remaining pitch control (right elevator) activity will generate rolling moment due to control asymmetry, (iii) some roll control required to compensate for roll asymmetries, thus available roll control power is reduced. The dynamic effects are only provided for pitch rate, and for the longitudinal components, i.e., normal force, axial force, and pitching moment due to body axis pitch rate. Because of the configuration asymmetry, an additional effect is provided, the rolling moment due to pitch rate. This would normally be zero and un-modeled for a symmetric configuration.

The L_1 adaptive controller response to the elevator loss from the left stabilizer is shown in Fig. 9. The α tracking is unaffected by the loss of left elevator; the right elevator segments compensate for the loss of pitch control power. The ailerons and rudder compensate for the induced rolling moment. For the given command magnitudes, the roll rate and β tracking are also unaffected by the elevator damage.

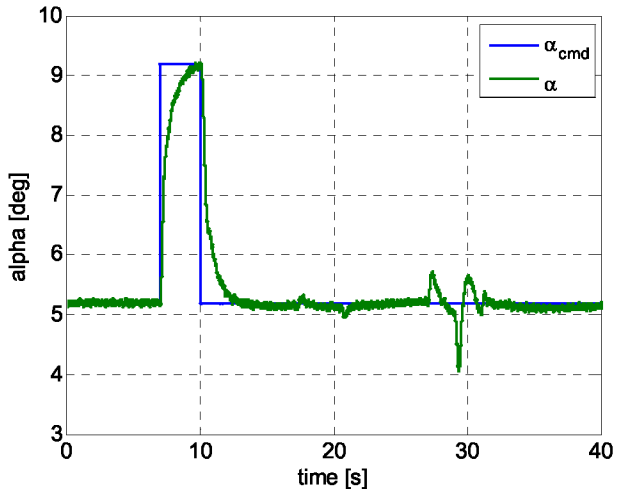

(a) Angle of attack

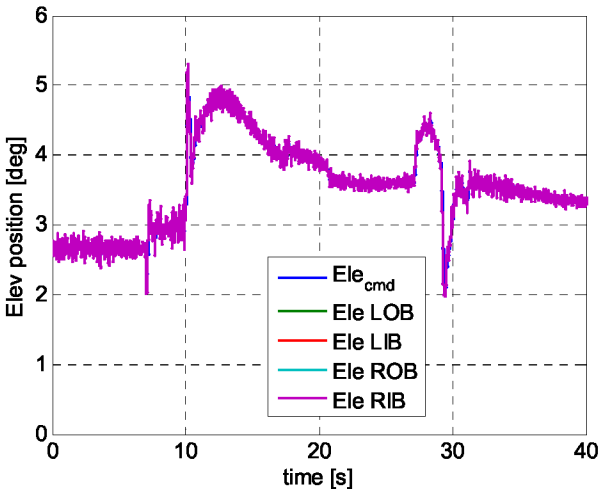

(b) Elevator

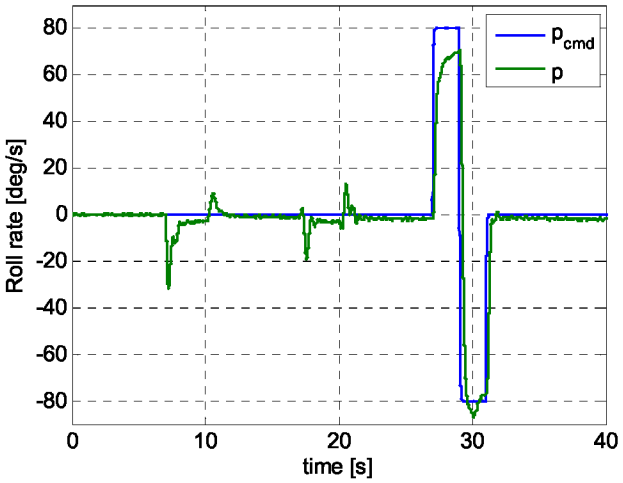

(c) Roll rate

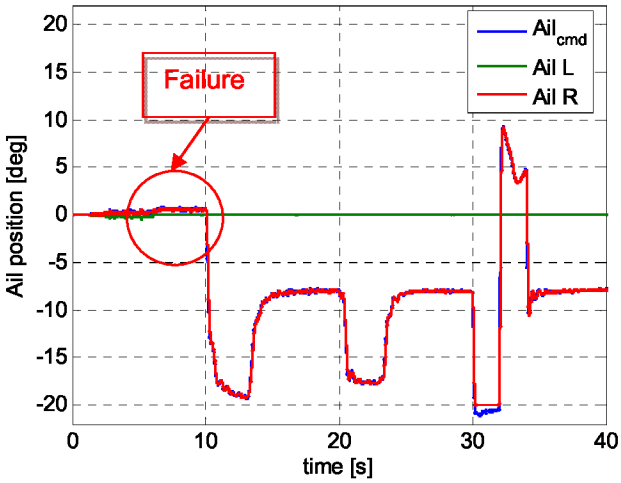

(d) Aileron

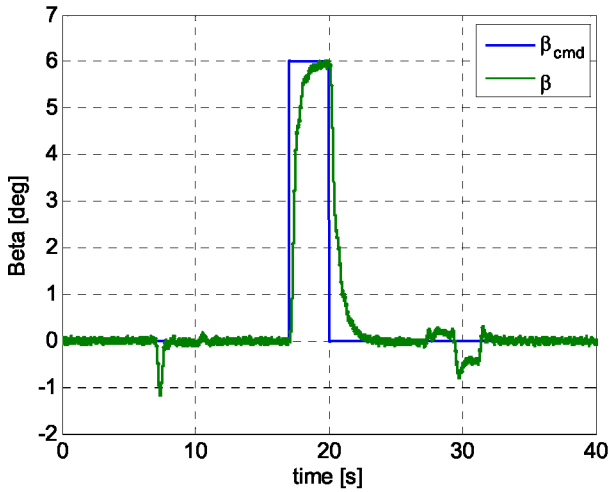

(e) Sideslip angle

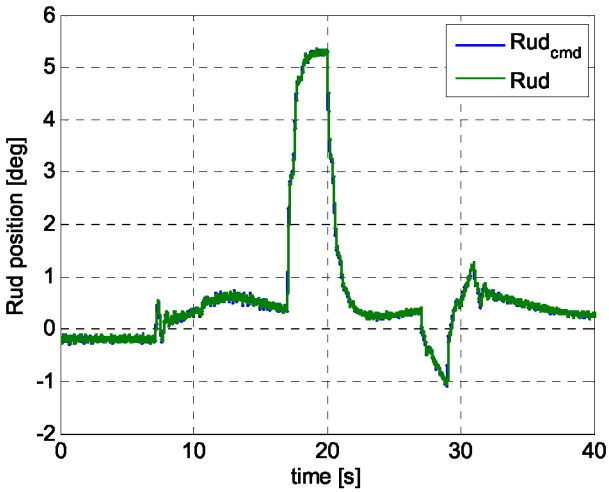

(f) Rudder

Figure 8. 25% semi-span left wing loss - α, p, β responses.

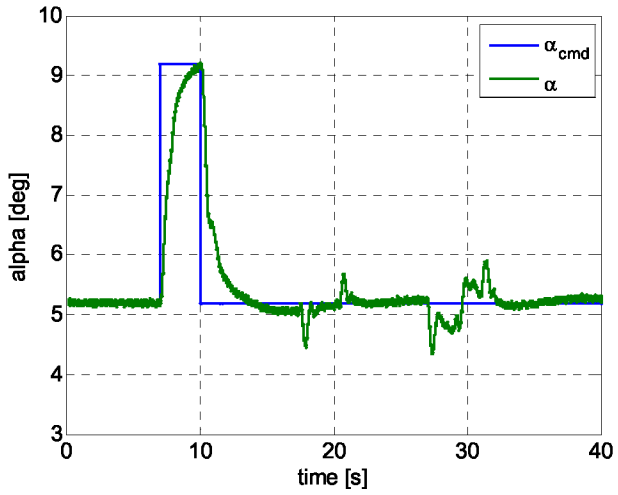

(a) Angle of attack

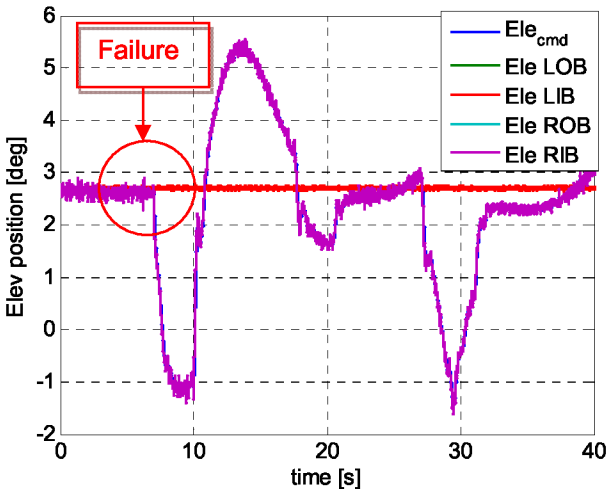

(b) Elevator

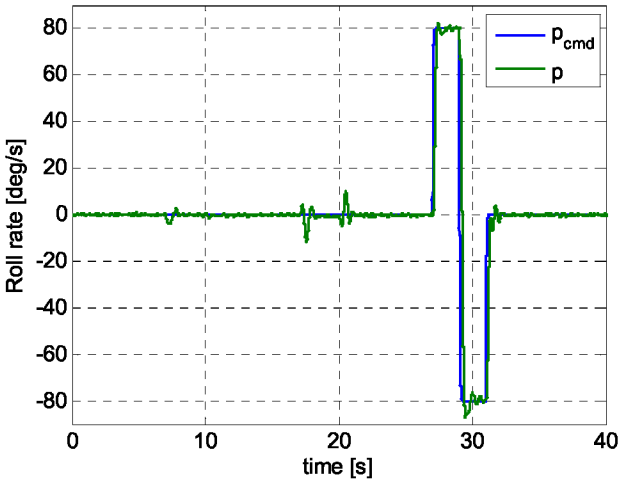

(c) Roll rate

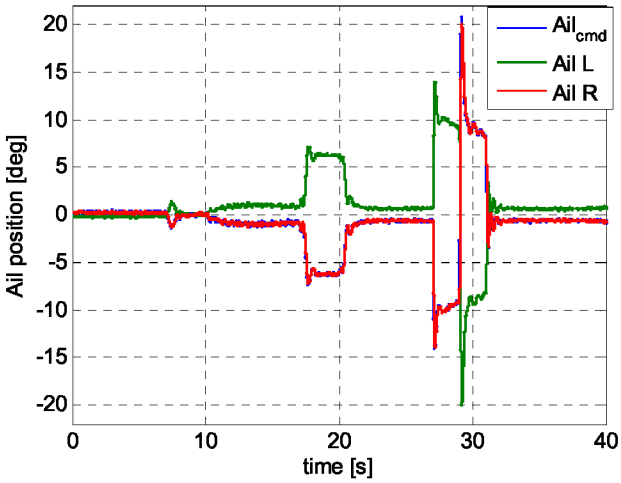

(d) Aileron

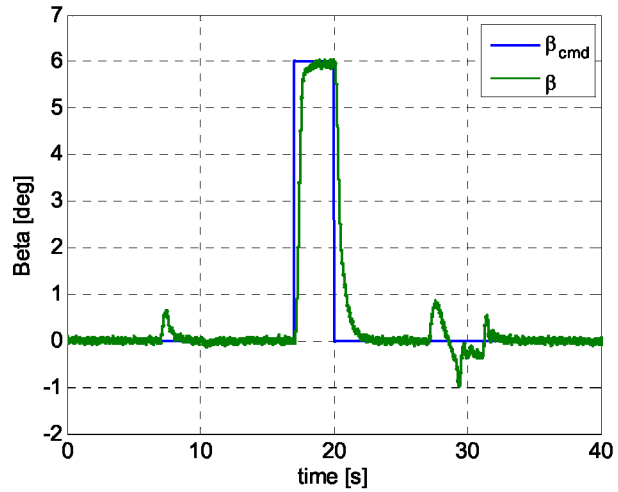

(e) Sideslip angle

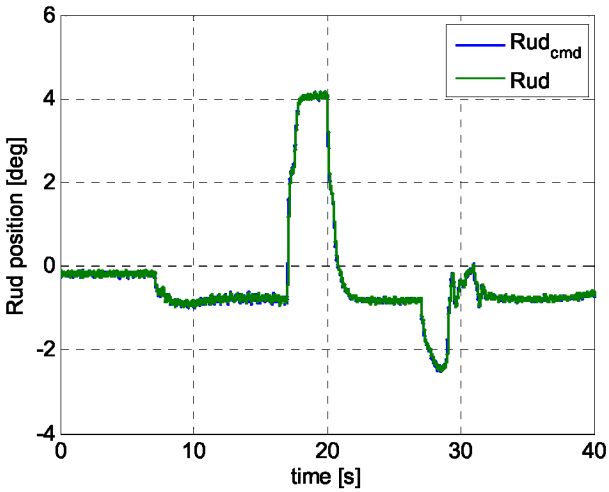

(f) Rudder

Figure 9. Entire elevator loss from left stabilizer - α, p, β responses.

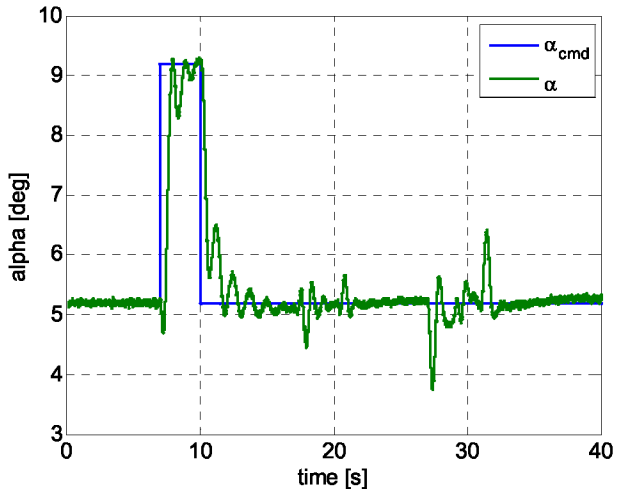

(a) Angle of attack

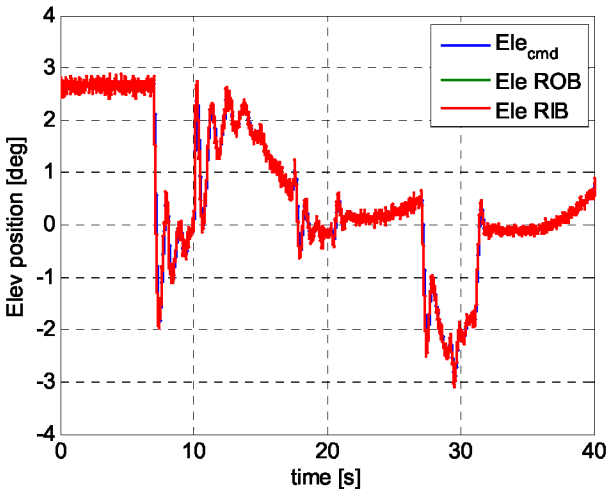

(b) Elevator

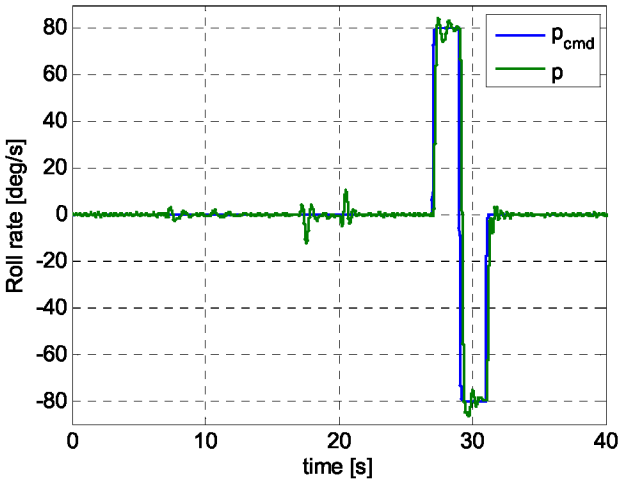

(c) Roll rate

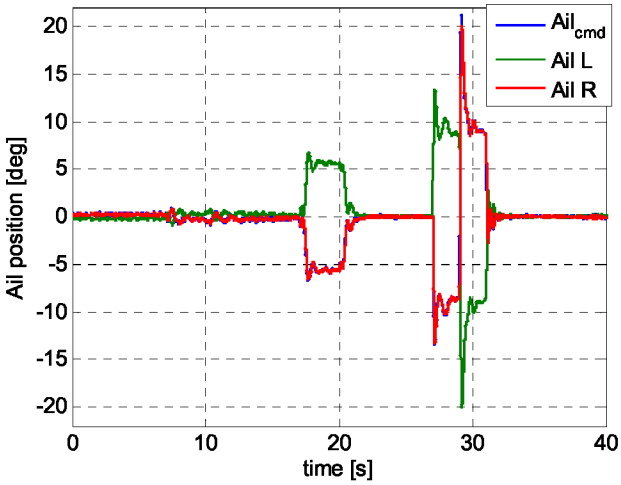

(d) Aileron

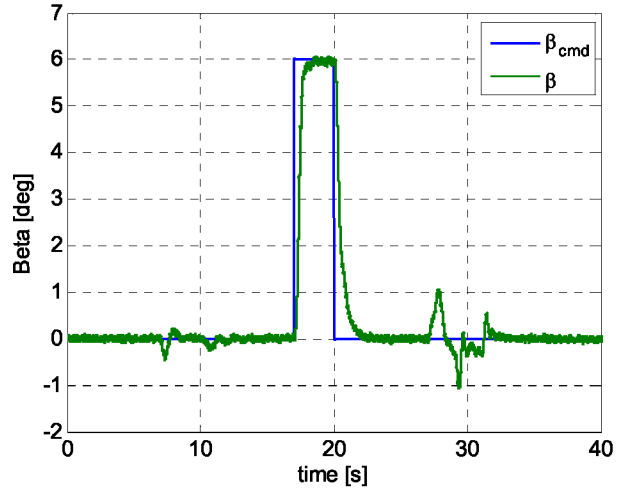

(e) Sideslip angle

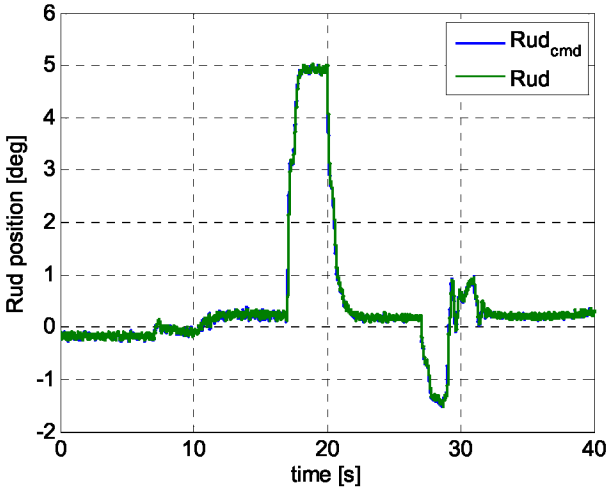

(f) Rudder

Figure 10. Entire left stabilizer loss - α, p, β responses.

Case 6: Damage case 6 – Loss of entire left stabilizer

The primary aerodynamic effects are reduction in longitudinal stability and rolling moment bias left wing down (-ΔCl), increases with α; the primary control effects are (i) reduction in pitch control power, all effects due to left elevator deflection go to zero, (ii) remaining pitch control (right elevator) activity will generate rolling moment due to control asymmetry, (iii) some roll control required to compensate for roll asymmetries, thus available roll control power is reduced. The dynamic effects are only provided for pitch rate, and for the longitudinal components, i.e., normal force, axial force, and pitching moment due to body axis pitch rate. Effects are modeled as being symmetric with direction of motion (positive versus negative rate). Because of the configuration asymmetry, an additional effect is provided, the rolling moment due to pitch rate. This would normally be zero and un-modeled for a symmetric configuration.

The L_1 adaptive controller response to the loss of entire left stabilizer is illustrated in Fig. 10. The α tracking performance is compromised by the stabilizer loss, becoming oscillatory. The right elevator segment compensates for loss in pitch control authority as well as induced rolling moment; additional correction from the ailerons is minimal during α tracking as can be seen form Fig. 10. There is a small deflection from the rudder to help with induced rolling moment. The roll rate and β tracking are unaffected by stabilizer failure.

Remark: A number of failure case have not been shown since the closed loop vehicle response is the same as the nominal aircraft. The cases presented represent the worse degradation in performance due to failure or damage. In some cases, there is no control power remaining to execute commanded maneuvers, in others the answer is not that clear and warrants further investigation.

B. Piloted Simulation

The piloted tasks were part of development and finalization of flight test tasks. The tasks were flown with no training or repeatability and thus are considered a preliminary evaluation. The GTM aircraft has three flight control modes as mentioned as shown in Fig. 3. Mode 1 is the revisionary stick to surface control, the aircraft is Level 1 in this configuration; Mode 2 is referred to as the Baseline control law and is an α-command, p-β stability augmentation system; Mode 3 is the research control law which is the L_1 adaptive α, p-β command control presented here. The Baseline α-command is an LQR PI based and is designed to operational limit of $\alpha \leq 10°$. It currently serves as the operational baseline feedback control law for the GTM. Hence, comparison between the L_1 and the Baseline α-command can be only performed for $\alpha \leq 10°$, comparisons for higher α range are performed with the stick to surface control law (Mode 1).

Task 1 – Angle of attack capture, static stability degradation

The task is trim at V=80 KEAS and Alt = 1200 ft. and then capture α=8° within 1 second, hold for 2 seconds, with α desired ±1°, α adequate ±2°. This task is repeated for various levels of static stability expressed as $\Delta Cm\alpha$ and ranging from 0 to 100%, i.e. from nominal stable aircraft to neutral static stability. This longitudinal task has been evaluated for the L_1 adaptive control law and the Baseline, both of which are α-command response type. The change in $\Delta Cm\alpha$ is achieved by using both inboard elevator sections, scheduled with α, to produce destabilizing effect. These two elevator sections also become unavailable to the control law. In a sense, it is a double fault – a destabilized aircraft and reduction in control power in the affected axis. The performance of both control laws is provided in Fig. 11 .

For nominal GTM aircraft, performance of both control laws is very similar, as illustrated in Fig. 11 (a)-(b), and a solid Level 1 flying qualities (FQ) according to pilot comments. However, as the static stability is decreased by 50%

(Fig. 11 (c)-(d)), the performance of the Baseline controller degrades to high Level 2 (Cooper-Harper rating 4) while the L_1 adaptive controller remains solid Level 1 FQ. With $\Delta C_{m\alpha} = 75\%$ (Fig. 11 (e)-(f)), the L_1 adaptive controller remains predictable and Level 1, while the Baseline performance degrades to achieving only adequate performance (Level 2, CHR 5). At the point of neutral static stability (Fig. 11 (g)-(h)), the L_1 adaptive controller is still described as predictable but does experience some oscillations and its performance is reduced to high Level 2 (CHR 4), while the Baseline controller is described as PIO prone and FQ are reduced to Level 3 bordering on uncontrollable CHR 10. One point we would like to emphasize is that the performance of the L_1 adaptive control law was found predictable by the pilot for all levels of static stability.

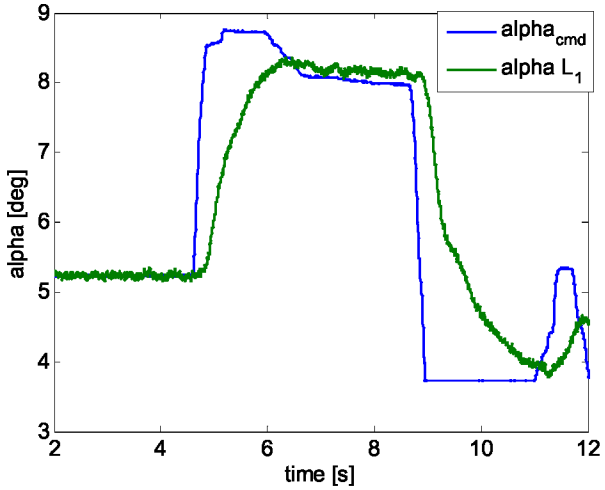

(a) $\Delta C_{m\alpha} = 0\%$ - L_1 adaptive

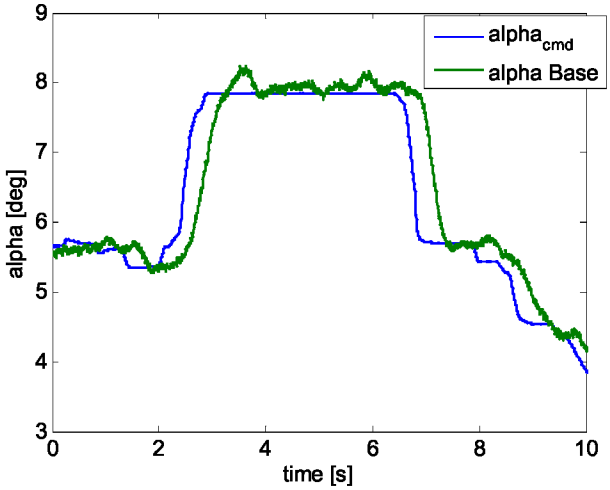

(b) $\Delta C_{m\alpha} = 0\%$ - Baseline

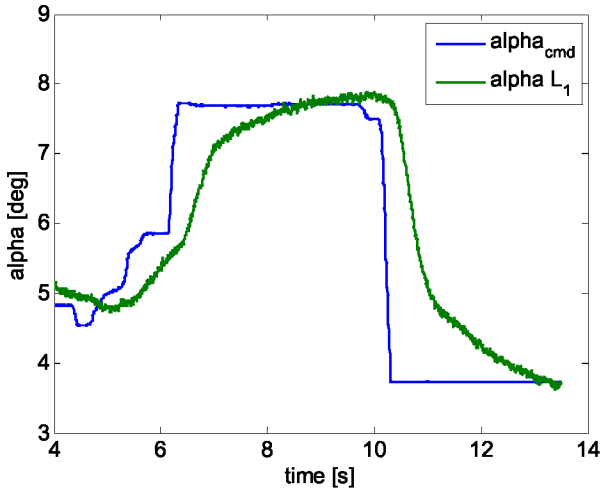

(c) $\Delta C_{m\alpha} = 50\%$ - L_1 adaptive

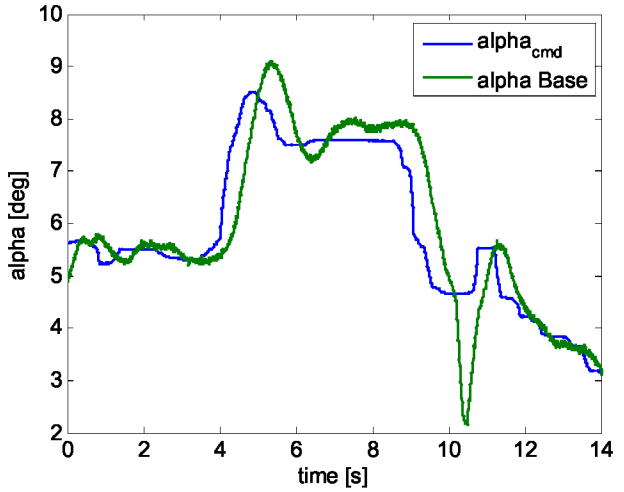

(d) $\Delta C_{m\alpha} = 50\%$ - Baseline

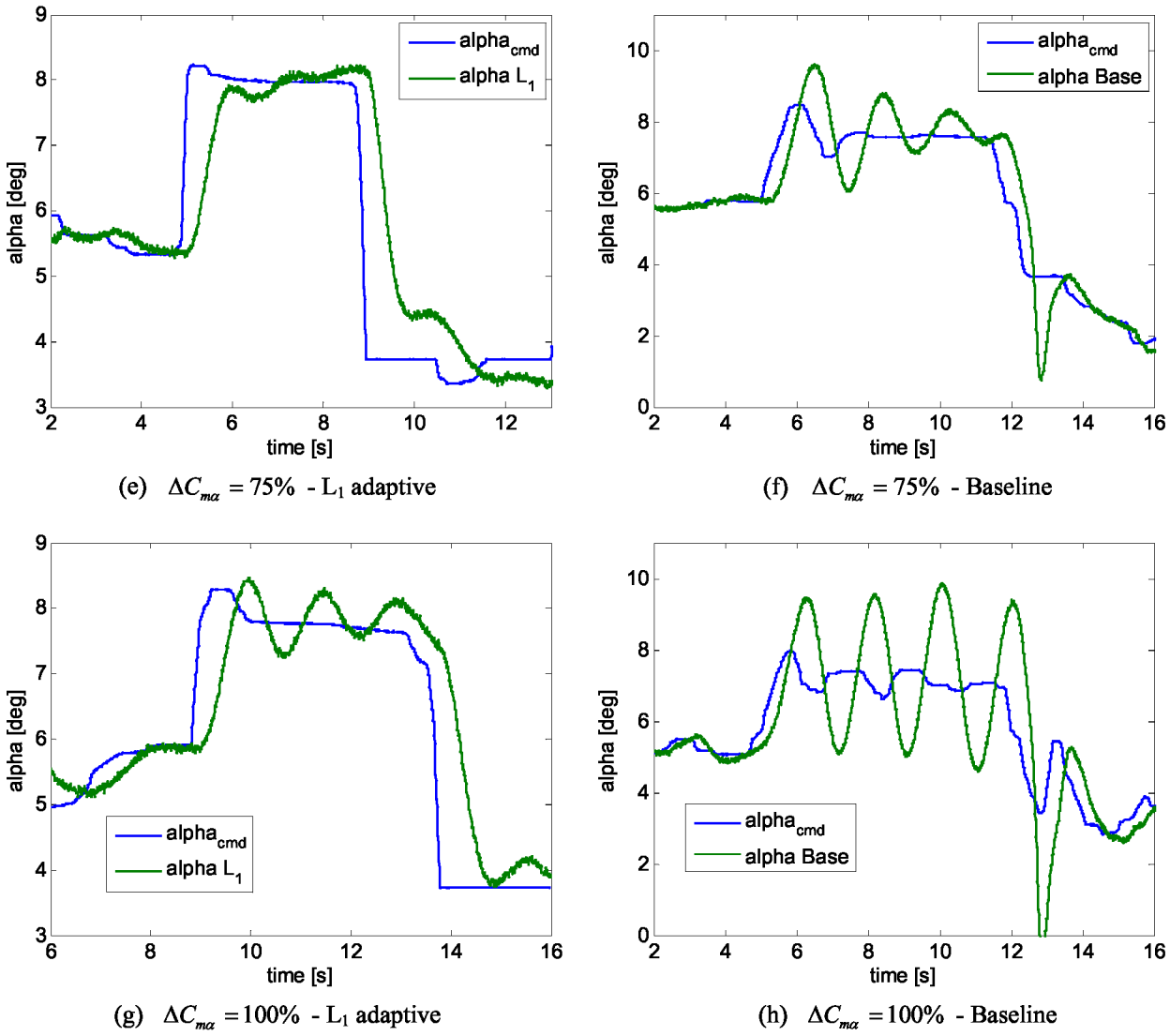

(e) $\Delta C_{m\alpha} = 75\%$ - L_1 adaptive

(f) $\Delta C_{m\alpha} = 75\%$ - Baseline

(g) $\Delta C_{m\alpha} = 100\%$ - L_1 adaptive

(h) $\Delta C_{m\alpha} = 100\%$ - Baseline

Figure 11. Angle of attack capture task with variable static stability.

Task 2 – Bank angle capture, roll damping degradation

The task is to trim at *V*=80 KEAS and *Alt* = 1200 ft. and then capture bank angle, ϕ=45° in 2 seconds, hold for 2 seconds, with ϕ desired ±5°, ϕ adequate ±15°. This task is repeated for various levels of roll damping expressed as ΔClp and ranging from 0 to 125%, unstable roll damping. This lateral-directional task has been evaluated for L_1 adaptive control law and the Baseline control law. The variation in ΔClp is produced by scheduling slats with α. The performance of both control laws is provided in Fig. 12 .

The plots in Fig. 12 show roll rate command (p_{cmd}), roll rate (p) and the resulting bank angle (ϕ). Since the Baseline control law is only a stability augmentation system in the lateral-directional axis, the roll rate command is an equivalent quantity derived from a lateral stick deflection. Since L_1 adaptive control law is a p-b command response type, roll rate command comes out naturally. The variable for comparison between the Baseline and the L_1 adaptive control laws in Fig. 12 is the bank angle. Pilot's comments are all related to the bank angle performance.

Both control laws are rated as providing Level 1 FQ for the nominal aircraft (Fig. 12 (a)-(b)). Furthermore, in both cases the Clp reduction by 50% was not apparent (Fig. 12 (c)-(d)). The differences between the two control laws become apparent at 75% Clp reduction. With the L_1 adaptive controller, the pilot achieves desired performance with low to moderate workload (Fig. 12 (e)), while that is no longer the case with the Baseline SAS (Fig. 12 (f)). In fact, the Baseline controller does not achieve adequate performance, has low damping and big overshoot. The difference between the two control laws is even more apparent for neutral roll damping as illustrated in Fig. 12 (g)-(h). The L_1 adaptive controller achieves desired performance with moderate workload, which makes it high Level 2 FQ (CHR 4). The Baseline controller on the other hand is considered unstable and uncontrollable, CHR 10. In this case, the L_1 adaptive controller provides a stable Level 2 FQ aircraft while the Baseline controller results in an uncontrollable. For ΔClp = 125%, negative roll damping, the L_1 adaptive controller degrades but is still stable.

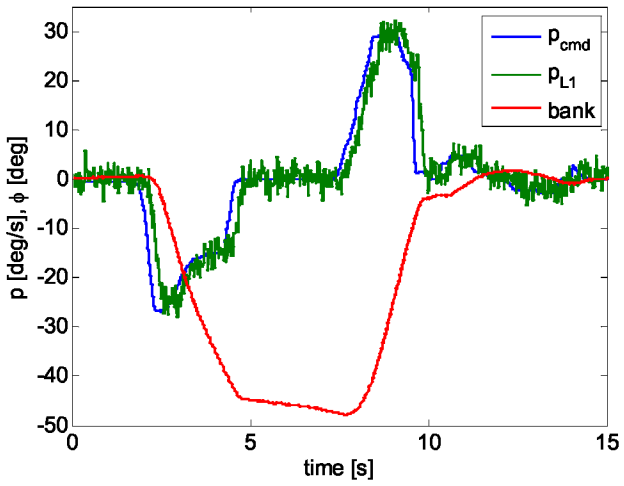

(a) $\Delta C_{lp} = 0\%$ - L_1 adaptive

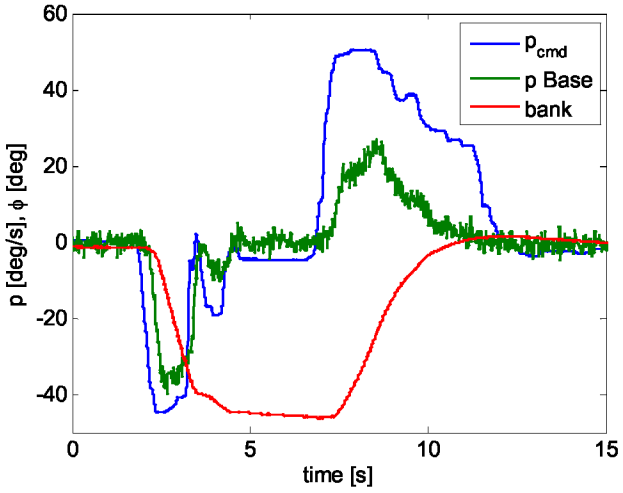

(b) $\Delta C_{lp} = 0\%$ - Baseline SAS

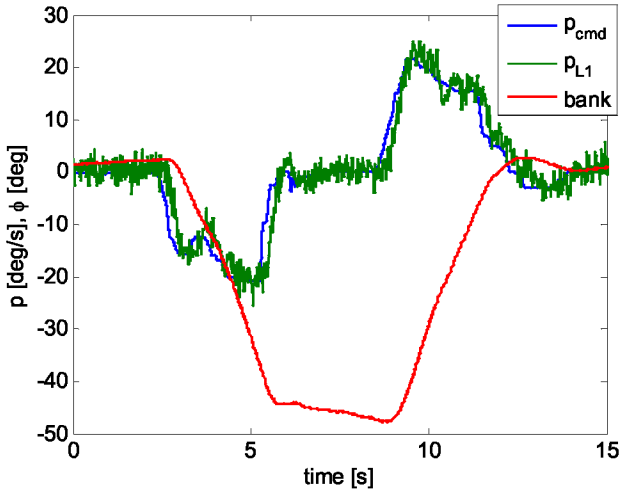

(c) $\Delta C_{lp} = 50\%$ - L_1 adaptive

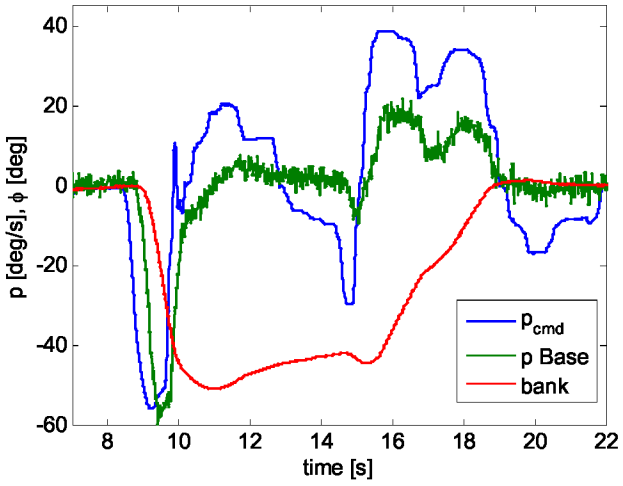

(d) $\Delta C_{lp} = 50\%$ - Baseline

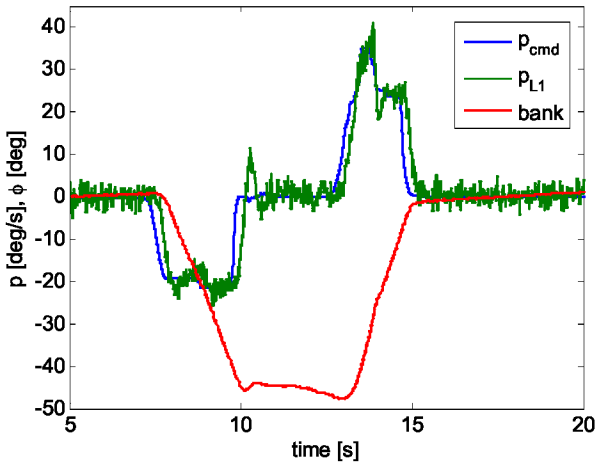

(e) $\Delta C_{lp} = 75\%$ - L_1 adaptive

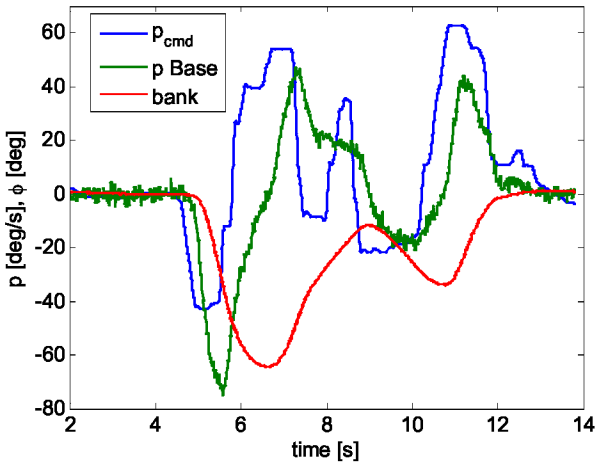

(f) $\Delta C_{lp} = 75\%$ - Baseline SAS

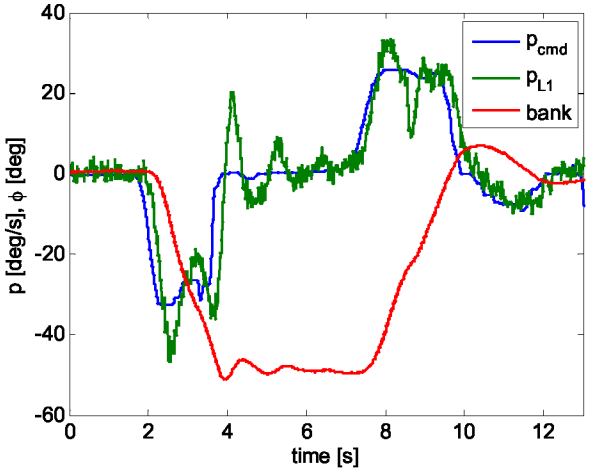

(g) $\Delta C_{lp} = 100\%$ - L_1 adaptive

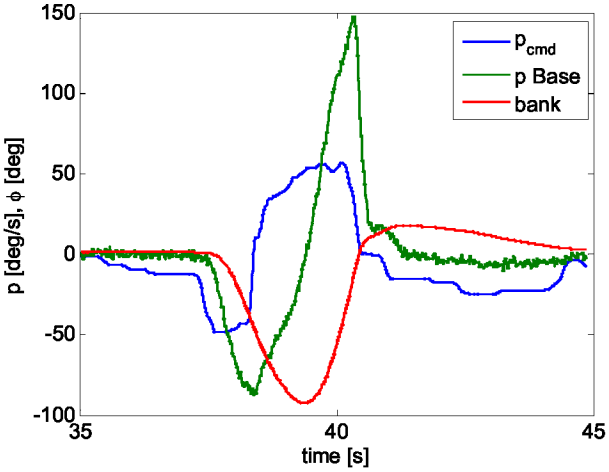

(h) $\Delta C_{lp} = 100\%$ - Baseline SAS

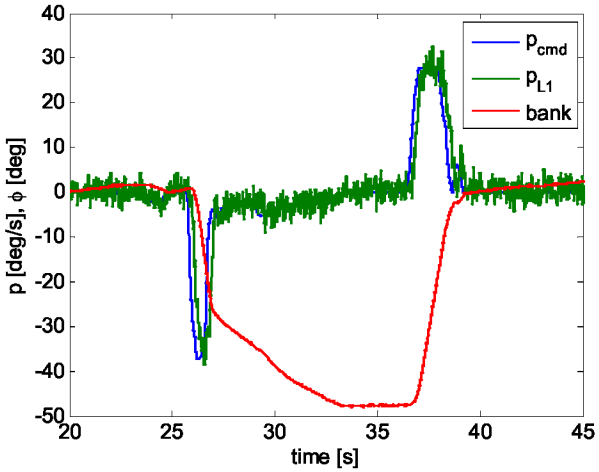

(i) $\Delta C_{lp} = 125\%$ - L_1 adaptive

Figure 12. Bank capture task with variable roll damping

Task 3 – Tight S-turns, simultaneous static stability and roll damping degradation

Tight S-turns maneuvers are part of a development for an offset landing task to be flown during the next flight test. This task is a demanding lateral task that would expose any potential issues with a control law. Since this is part of a larger task, no assessment criteria specific to the S-turn execution has been developed. The pilot's evaluation focused on how easily and precisely he could execute these turns. Aircraft dynamics were varied during this task by simultaneously altering $\Delta Cm\alpha$ and ΔClp from 0% to 100%, thus turning the vehicle from nominal to statically neutrally stable with zero roll damping. The proposed flight cards for this task have the following notes that are indicative of how demanding the task is: $\Delta Cm\alpha/Clp$=50% Loss of Control (LOC) possible; $\Delta Cm\alpha/Clp$=75% LOC probable; $\Delta Cm\alpha/Clp$=100% LOC likely.

One item to note for this task flown with the Baseline and the L_1 adaptive controllers is how much uncertainty can be tolerated by each control law. Due to insufficient evaluation criteria, performance comparison between the two controllers and within the controller for changing stability is difficult to make. Hence, we consider qualitative performance for bank angle for varying degree of deviation from the nominal vehicle. Fig. 13 (a) shows the performance of the L_1 adaptive controller for $0\% \leq \Delta Cm\alpha/Clp \leq 100\%$. For $0\% \leq \Delta Cm\alpha/Clp \leq 75\%$ the L_1 adaptive controller provides predictable performance at high Level 2 or better FQ. For zero roll damping and neutral static stability, tight S-turn execution is difficult to perform but not unstable according to the pilot. For the $\Delta Cm\alpha/Clp$=0%, 50% cases, the Baseline control law provides reasonable bank angle performance in the high Level 2- Level 1 FQ (Fig. 13 (b)). However, at $\Delta Cm\alpha/Clp$=75% the aircraft is deemed uncontrollable by the pilot

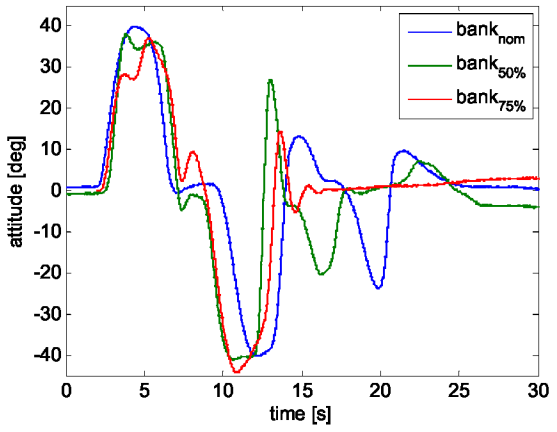

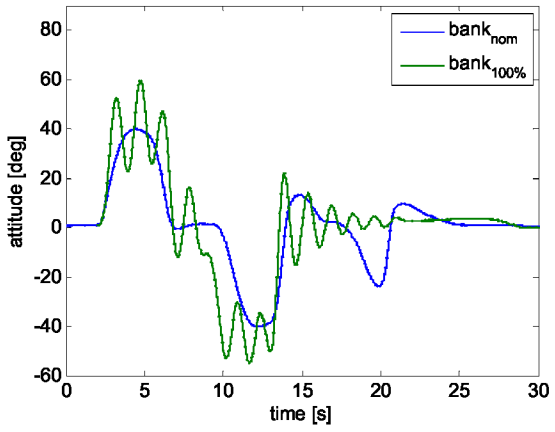

(a) L_1 adaptive control

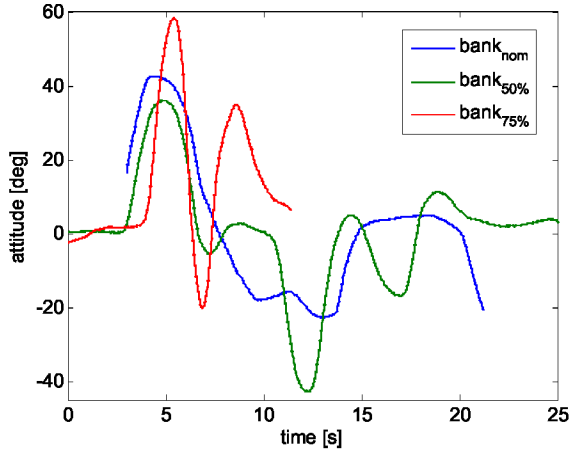

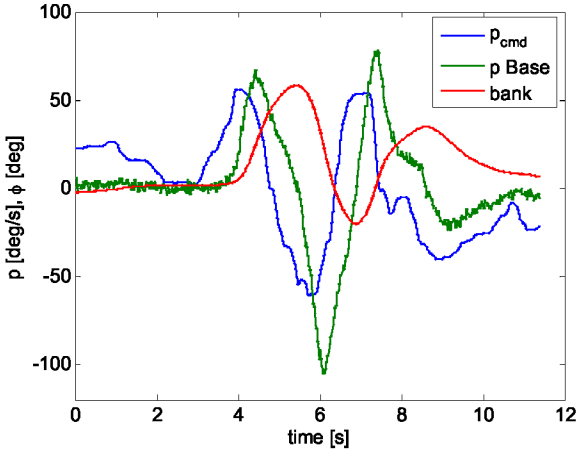

(b) Baseline controller – uncontrollable at $\Delta Cm\alpha/Clp$ = 75%

Figure 13. Offset landing task – tight S-turns

Task 4 – High angle of attack capture task

One of the several research objectives for the AirSTAR facility is to identify high angle of attack dynamics and verify these against obtained wind tunnel and CFD data. In order to do so, the GTM aircraft flight must be able to safely fly at the very edges of attainable flight envelope. Part of the upcoming flight test is the high α envelope expansion. In addition, the GTM exhibits highly nonlinear phenomena for $12°\leq\alpha\leq18°$ called "pitch break." In other words, if in open loop the aircraft reaches $\alpha=12°$, it will pitch up and could be recovered only once it reaches $\alpha=18°$. Thus the envelope expansion is envisioned flown in the revisionary stick-to-surface control mode with 2° α increments from $\alpha=18°$ to $\alpha=28°$. On the other hand, the L_1 adaptive controller is expected to perform α capture task for entire post-stall region starting at $\alpha=12°$.

The aerodynamics in the post-stall region are nonlinear and increasingly asymmetric with increased α. For $12°\leq\alpha\leq20°$ the aerodynamics are expected to be asymmetric, the roll damping (Clp) is expected to be low, and nose roll off is also expected. Beyond $\alpha=28°$ n addition to aerodynamic asymmetry and low roll damping, a pronounced noseslice due $C_{n\beta}\approx0$ is expected. The α capture performance for the L_1 adaptive controller is illustrated in Fig. 14. The task is, starting in trim at V=80KEAS, to capture indicated α at the rate of 3 deg/sec, hold for 4 seconds, with α desired ±1°, α adequate ±2°. Note that desired and adequate criteria is the same as α capture in the linear region; additionally, holding for 4 seconds would expose any control law instability in this "pitch break" region. Due to the nature of expected dynamic behavior in the high α region, β and ϕ are additional variables of interest plotted in Fig. 14. The L_1 adaptive controller performance was judged as close to nominal α capture task. For $\alpha=20°$ case (Fig. 14 (b)), the approach was at high pitch rate with Vmin getting into the 30's (KEAS); this created some nascent small oscillations as α approached 20°. The $\alpha=26°$ case was performed less rapidly and the slight oscillations are no longer present (Fig. 14 (c)). For comparison purposes, the same α case for the revisionary stick to surface controller is shown in Fig. 14 (d). Note the oscillatory nature of α as it follows the ramping α_{cmd}, also note the bank and β excursions which illustrates the expected roll off (ϕ) and noseslice (β) dynamics. Fig. 15 provides another way of looking at the high α capture task by illustrating the coupling between these variables. Ideally, an α excursion would be completely decoupled from β and would produce a straight vertical line on the plot. The L_1 adaptive controller produces $|\beta|\leq1°$ excursions, as shown on Fig. 15 (a). On the other hand, the revisionary stick to surface control law shows significantly greater degree of coupling between the α–β axis as illustrated in Fig. 15 (b).

Task 5 – Sudden asymmetric thrust

This maneuver was performed unrehearsed once for each control law – reversion stick to surface mode and L_1 adaptive controller. The results of this maneuver are used for qualitative comparison between the two control law responses with pilot in the loop and no training. The task starts the airplane climbing at 30° attitude and throttles at full power, then at some the left throttle is reduced from 100% to 0-% thrust. This is primarily a lateral-directional task since the sudden change in thrust induces rolling moment affecting ϕ and side force affecting β. The ϕ–β coupling induced by asymmetric thrust for both control laws is illustrated in Fig. 16. Note that the L_1 adaptive controller minimizes the rolling moment and allows for stable and rapid β recovery.

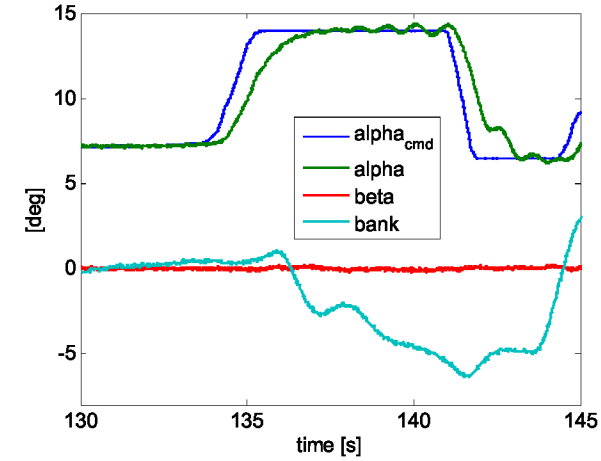

(a) $\alpha_{cmd} = 14°$

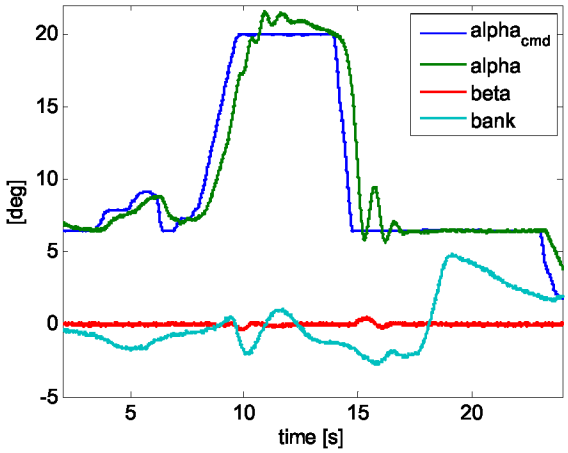

(b) $\alpha_{cmd} = 20°$

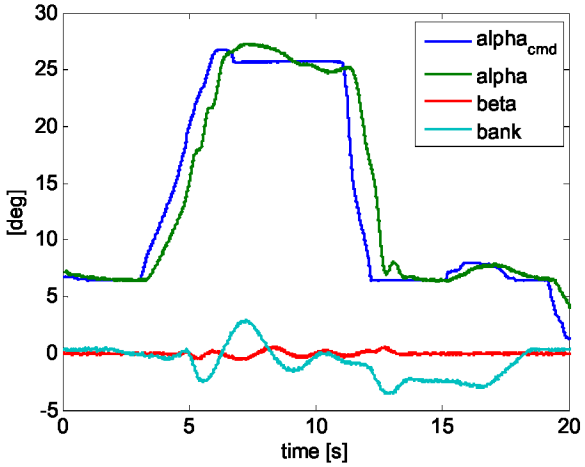

(c) $\alpha_{cmd} = 26°$ L_1 adaptive

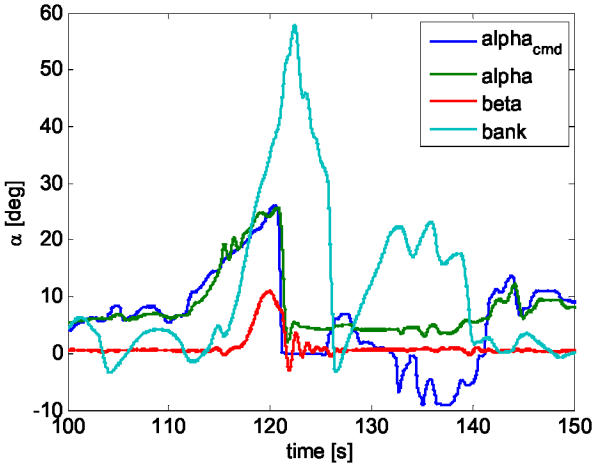

(d) $\alpha_{cmd} = 26°$ stick-to-surface control

Figure 14. High α capture task

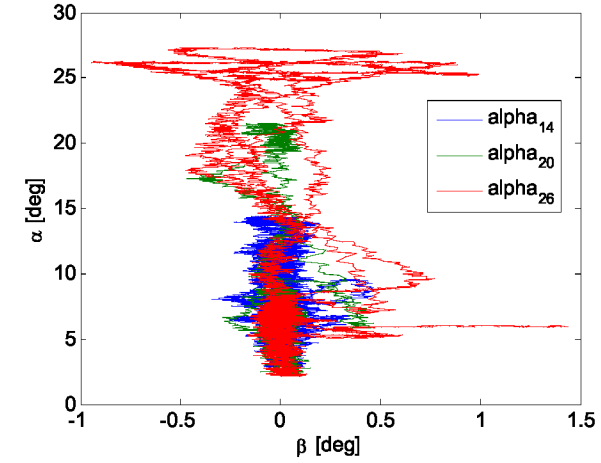

(a) L_1 high α range

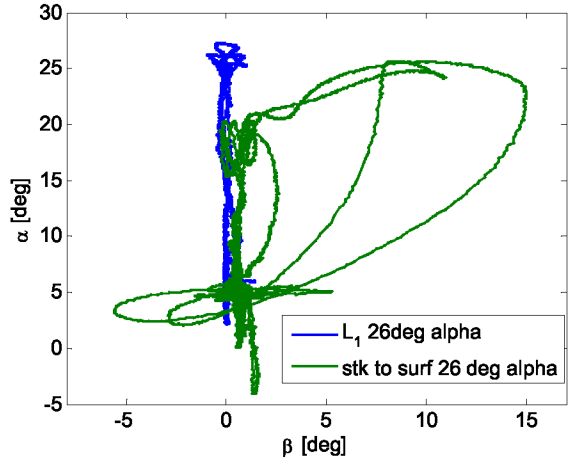

(b) L_1 vs. stick to surface control α=26

Figure 15. α–β excursions for high α task

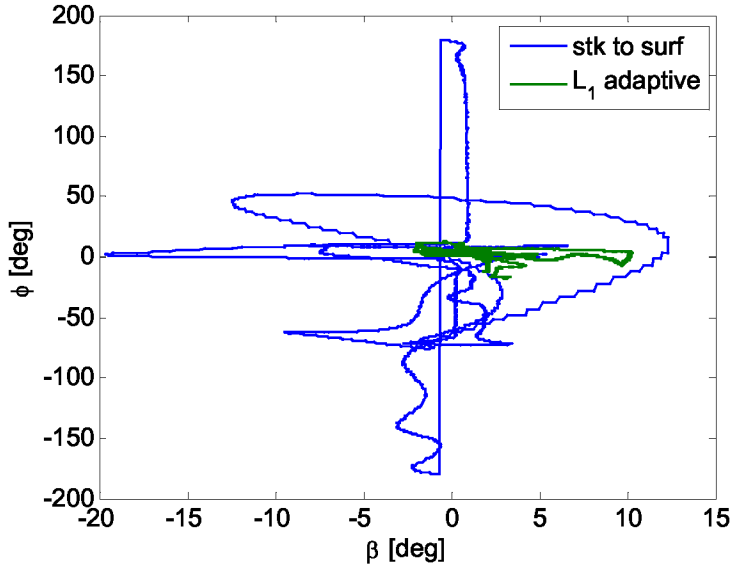

Figure 16. Asymmetric engine out

Task 6 – Pilot induced upset and recovery

Another unrehearsed maneuver performed for quantitative control law assessment is a pilot induced upset and recovery to determine whether the L_1 adaptive controller prevents the pilot from executing the maneuver. At approximately 28 seconds the pilot induces upset by applying full rudder and opposite lateral stick, and then holds it for 6 seconds (Fig. 17 (a)). At the end of 6 seconds interval the pilot attempts to recover the aircraft by reducing α to 8° and stabilizing roll. As seen in Fig. 17 (b), with the L_1 adaptive controller in the loop the pilot rapidly reduces α to approximately 5° and stabilizes roll to less than 10° within 10 seconds of initiating the recovery maneuver. Thus, the L_1 adaptive controller does not prevent the pilot from recovering the aircraft from an upset. Whether the controller has assisted the pilot in this task will be further investigated.

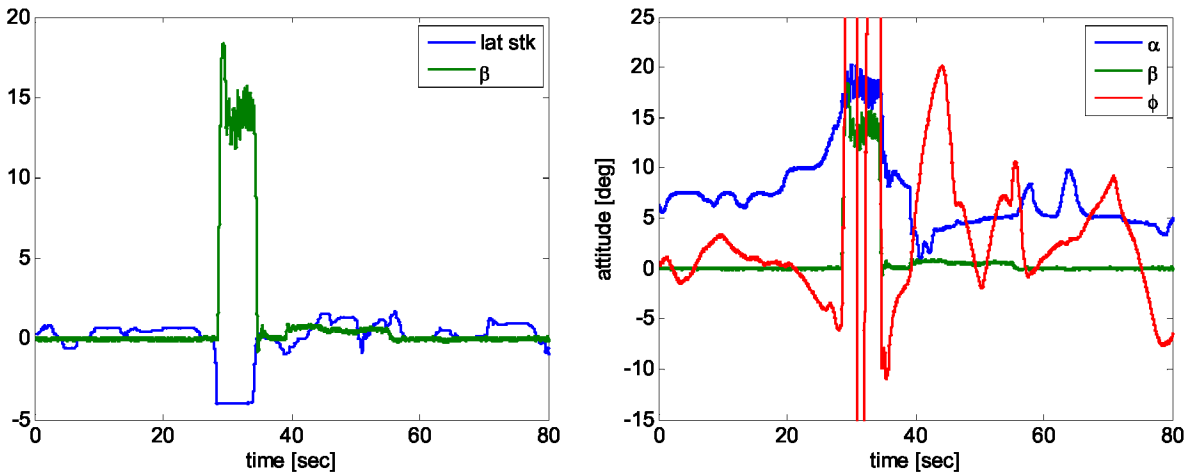

(a) Upset inducing maneuver (b) Upset and upset recovery

Figure 17. Induced upset recovery (hard rudder + opposite stick and hold for 6 seconds)

V. Conclusions / Future Plans

We have presented the L_1 adaptive controller for unmatched uncertainties and its application to the AirSTAR GTM nonlinear simulation. The controller was designed at a single flight condition in the heart of the nominal flight envelope. The analysis was performed for variable dynamics and damage cases in the highly nonlinear areas of the flight envelope, in both batch and piloted evaluation. These analysis and evaluations were performed in preparation for delivering the L_1 adaptive control law to be flight tested on the GTM, part of the AirSTAR facility. Future work will entail flight testing the L_1 adaptive controller and comparing those results to the ones obtained in the piloted simulation.

VI. Acknowledgments

The authors would like to acknowledge the staff of the AirSTAR Flight Test Facility for their support with control law implementation, their insights into flight dynamics and piloted evaluations.

VII. References

[1] Foster J. V., Cunningham K., Morelli E. A., and Murch A. M., "Practical Application of a Subscale Transport Aircraft for Flight Research in Control Upset and Failure Conditions," AIAA 2008-6200, AIAA Atmospheric Flight Mechanics Conference, Honolulu, HI, 2008.

[2] Murch, A. M., "A Flight Control System Architecture for the NASA AirSTAR Flight Test Infrastructure," AIAA 2008-6990, AIAA Guidance, Navigation, and Control Conference and Exhibit, Honolulu, HI, 2008.

[3] Murch, A. M., Cox, D.E, Cunningham K.," Software Considerations for Subscale Flight Testing of Experimental Control Laws," To be presented at The InfoTech@Aerospace 2009, Seattle, WA, April, 2009.

[4] Jordan, T. L., Foster, J. V., Bailey, R. M., and Belcastro, C. M., "AirSTAR: A UAV Platform for Flight Dynamics and Control System Testing,", AIAA 2006-3307, 25th AIAA Aerodynamic Measurement Technology and Ground Testing Conference, San Francisco, CA, 2006.

[5] Jordan, T. L., Langford, W. M., and Hill, J. S., "Airborne Subscale Transport Aircraft Research Testbed – Aircraft Model Development," AIAA 2005-6432, AIAA Guidance, Navigation, and Control Conference, San Francisco, CA, 2005.

[6] Bailey, R.M., Hostetler, R.W., Barnes, K.N., Belcastro, Christine M., and Belcastro, Celeste M., "Experimental Validation: Subscale Aircraft Ground Facilities and Integrated Test Capability," AIAA 2005-6433, AIAA Guidance, Navigation, and Control Conference, San Francisco, CA, 2005.

[7] Cao, C. and N. Hovakimyan, "Design and Analysis of a Novel L_1 Adaptive Control Architecture, Part I: Control Signal and Asymptotic Stability." Proc. of American Control Conference, pp. 3397-3402, 2006.

[8] Cao, C. and N. Hovakimyan, "Design and Analysis of a Novel L_1 Adaptive Control Architecture, Part II: Guaranteed Transient Performance." IEEE Trans. On Automatic Control, vol. 53, no. 2, pp. 586-591 March 2008.

[9] Cao, C. and N. Hovakimyan, "Guaranteed Transient Performance with L_1 Adaptive Controller for Systems with Unknown Time-varying Parameters and Bounded Disturbances." American Control Conference, pp. 3925-3930, 2007.

[10] Cao, C. and N. Hovakimyan, "Stability Margins of L_1 Adaptive Control Architecture." American Control Conference, pp. 3931-3936, 2007.

[11] Kaminer, I., Pascoal, A., Xargay, E., Cao, C., Hovakimyan, N., and Dobrokhodov, V., "3D Path Following for Small UAVs using Commercial Autopilots augmented by L_1 Adaptive Control," Submitted to Journal of Guidance, Control and Dynamics.

[12] Wise, K., E. Lavretsky, N. Hovakimyan, C. Cao, and J. Wang., "Verifiable Adaptive Flight Control: UCAV and Aerial Refueling," AIAA 2008-6658, AIAA Guidance, Navigation, and Control Conference, Honolulu, HI, 2008.

[13] Wang, J., C. Cao, N. Hovakimyan, R. Hindman and D.R. Ridgely, "L_1 Adaptive Controller for a Missile Longitudinal Autopilot Design," AIAA 2008-6282, AIAA Guidance, Navigation, and Control Conference, Honolulu, HI, 2008.

[14] Kharisov, E., I.M. Gregory, C. Cao and N. Hovakimyan, "L_1 Adaptive Control Law for Flexible Space launch Vehicle and Proposed Plan for Flight Test Validation," AIAA 2008-7128, AIAA Guidance, Navigation, and Control Conference, Honolulu, HI, 2008.

[15] Cao, .C and N. Hovakimyan, "L_1 Adaptive Output-Feedback Controller for Non-Strictly-Positive-Real Reference Systems: Missile Longitudinal Autopilot Design." Journal of Guidance, Control and Dynamics, vol. 32, no. 3, pp.717-726, May-June 2009.

[16] Murch, A. M., "Aerodynamic Modeling of Post-Stall and Spin Dynamics of Large Transport Airplanes," Master's Thesis, Georgia Institute of Technology, Atlanta, GA, 2007.

[17] Foster, J. V., K. Cunningham, C. M. Fremaux, G. Shah, E. Stewart, R. Rivers, J. Wilborn, and W. Gato, "Dynamics Modeling and Simulation of Large Transport Airplanes in Upset Conditions, AIAA-2005-5933, AIAA Guidance, Navigation, and Control Conference, San Francisco, CA, August 2005.

[18] Shah, G. "Aerodynamic Effects and Modeling of Damage to Transport Aircraft." AIAA-2008-6203 AIAA Guidance, Navigation, and Control Conference , Honolulu, HI, 2008.

[19] Wise, K.A., Lavretsky, E., Zimmerman, J., Francis, J.H., Dixon, D., and Whitehead, B., "Adaptive Flight Control of a Sensor Guided Munition," AIAA-2005-6385. AIAA Guidance, Navigation, and Control Conference, San Francisco, CA, August 2005.

[20] Sharma, M., E. Lavretsky, and K.A. Wise, "Application and Flight Testing of an Adaptive Autopilot on Precision Guided Munitions," AIAA-2006-6568, AIAA Guidance, Navigation, and Control Conference, Keystone, CO, August 2006.

[21] Beard, R., C. Cao, and N. Hovakimyan, "An L_1 Adaptive Pitch Controller for Miniature Air Vehicles," AIAA-2006-6777, AIAA Guidance, Navigation, and Control Conference, Keystone, CO, August 2006.

[22] Xargay, E., Hovakimyan, N. and C. Cao, L_1 Adaptive Controller for Nonlinear Systems in the Presence of Unmatched Uncertainties," submitted to the 2010 American Control Conference, June 20101, Baltimore, MD.

[23] MIL-STD-1797A, Anonymous, "Military Standard, Flying Qualities of Piloted Vehicles," 1990.